SCIENTIFIC COMMITTEE

NINETEENTH REGULAR SESSION

Koror, Palau

16-24 August 2023

Spatial structure and regional connectivity of bigeye and yellowfin tuna stocks in the WCPO derived from the reference SEAPODYM models

WCPFC-SC19-2023/SA-IP-06

28 July 2023

Inna Senina[1], John Hampton[1], Lucas Bonnin[1], Patrick Lehodey[1,2], Paul Hamer[1], and Simon Nicol[1]

[1]Oceanic Fisheries Programme (OFP), Pacific Community (SPC), Noumea, New Caledonia
[2]Mercator Ocean International, Toulouse, France

Contents

1. Executive summary

This information paper describes the spatial structure and movement patterns of yellowfin and bigeye tuna populations derived from two reference Pacific-wide SEAPODYM models, developed with the application of quantitative methods to estimate model parameters. Comparing the modelling results for these two large tropical tuna populations, the paper provides a general overview of each model configuration, the parameter estimates, validation, predicted spatial structure, fisheries impact, the consistency between SEAPODYM and MULTIFAN-CL estimates, and the results of the connectivity analysis. Since the regional movement probabilities were provided for the alternative models considered in the respective stock assessments, the objective of this paper is to inform the Scientific Committee on the main model properties, their consistency with observations, existing uncertainties, and the method to compute regional movement rates.

2. SEAPODYM reference models

In this Information paper, the models of yellowfin (*Thunnus albacares*) and bigeye (*Thunnus obesus*) tuna in the Pacific Ocean are summarized to facilitate understanding of the predicted spatial structure and the derived movement patterns. The development of the yellowfin model was presented in the earlier scientific reports (Senina et al., 2015; Lehodey, 2017) and the reference model was then used in the studies of the climate change impacts (Senina et al., 2018; Bell et al., 2020) including the study of the combined effects of ocean warming and acidification on the larval mortality of yellowfin tuna (Nicol et al., 2022). In the model of yellowfin, only the catch and length frequency data were included in the likelihood function, while the tagging data were used in the tag movement model to obtain the optimal values of habitat and movement parameters, which were then used to define the range of variation of corresponding parameters and to set their initial values in the optimization experiments. In the bigeye model, the catch, length frequency of catch and the tagging data were used in the full likelihood context. The bigeye model configuration and the reference model development are fully described in Senina et al. (2020, 2021). The CLT (Catch, Length and Tagging data) model maximum likelihood solution was recently updated with the objective to improve the estimates of early life stages and juvenile dynamics as well as to revise the estimates of natural mortality, which showed a persistent bias in the fit to the length frequency data in the previous solution (Senina et al., 2021). This Information paper presents the updated modeling results.

2.1 Configurations of the reference models

The SEAPODYM model configuration includes the definitions of 1) the spatiotemporal and age resolution of the numerical model, 2) the modelling time period, 3) the forcing datasets, 4) the observational datasets, and 5) the model parameters, both fixed and estimated. Table 1 summarizes the details of the configuration of (1-3). Note, that the time range in the optimization is shorter than the modelling time period due to the need to leave the data for validation and to "forget" the initial conditions at the beginning of optimization runs. Also, the MLE solution for the yellowfin model was downscaled to a higher 1° resolution, which explains why it is available at two spatial resolutions (Table 1).

For both species, the geo-referenced catch data (Figure 1) were consistent with the total landings data, which is important in order to account for 100% of fishing mortality. The fisheries data were structured into SEAPODYM fisheries (see Table A2 in Senina et al., 2018 and Table 1 in Senina et al., 2021). The tagging data that were used in the preliminary optimization experiments in the yellowfin model development are fully described in (Senina et al., 2015).

The configuration of the tagging data in the bigeye model optimizations can be seen in (Senina et al., 2020b). The selected dataset, the spatial distribution and the length distributions, used in optimizations and validation are shown in Figure 2. As previously, the sub-set of tagging data from 2000 to 2007 was left for model validation, while the 2008-2014 sub-set was used in the optimizations.

The fixed model parameters, used in the reference model configurations (Figure 3), include the mean length and weight at age and maturity-at-age profiles. The growth model of yellowfin tuna was taken from the stock assessment report (Langley et al., 2011) and is consistent with earlier works (Lehodey and Leroy, 1999; Hampton, 2006). For bigeye tuna, two growth models (Harley et al., 2014 ; Ducharme-Barth et al., 2020) were tested in the reference model development, and the model used in Harley et al. (2014) that reflects mainly the growth of bigeye tuna in the EPO was selected for its best performance in terms of validation scores and parameter estimates. The mean ages of the monthly age classes (see Table 1) were used to obtain the mean sizes in SEAPODYM. The age structure in SEAPODYM is further structured into life stages as follows: one monthly age class of larvae, 2 monthly classes of small juveniles and the rest of age classes were defined as juveniles (immature) and mature adults according to the maturity profile. As seen from Figure 3 (left panel), in the yellowfin model the step function of maturity was used, assuming all individuals in the population become reproductive capable at the age of 20.5 months. The bigeye model configuration uses the smooth maturity function as in the recent MULTIFAN-CL model (Ducharme-Barth, 2020).

2.2 Parameter estimates

All biological parameters defining the dynamic rates of reproduction, mortality, movement, and the habitat indices are listed in Table 2 and the corresponding links to the environmental variables are shown in Figure 4. It is worth noting the major differences between spawning and feeding habitat parameter estimates for yellowfin and bigeye tunas. Thus, the preferred temperature range for yellowfin larval habitat is estimated to be narrower and 3.5°C higher than that of bigeye, with optimum temperatures being 29°C and 25.5°C respectively. Similarly, the prey and predator functions are estimated to be very different, showing higher sensitivity of yellowfin larvae survival to prey and predator densities, while bigeye larvae survival is strongly affected by the density of predators, and sensitive only to the very low concentrations of prey organisms (Figure 4, panel Reproduction). These estimations are also explained in the forms of the frequency distributions of the species' larvae with respect to environmental variables (Figure 5).

The parameters of natural mortality function could be estimated for yellowfin, thanks to a longer modelling times and the optimization time period, 1986-2010, covering three life spans of the species (Table 1). Besides, the instantaneous mortality rates are estimated to vary with environmental conditions, so the effective mortality rates, computed as the global averages weighted by the population density at age, are substantially higher than theoretical ones given by the assumed mortality function, thus ranging between 0.018 mo^{-1} and 0.226 mo^{-1}. In the reference bigeye model, the choice had to be made between estimation of reproduction and mortality parameters due to short modelling times, including only 1.5 life spans of the species life span in the optimization, with the data from 2003 to 2017 (Table 1), and the resulting correlation between these two groups of parameters. The mortality function parameters were calibrated to provide the best fit to the length frequency data, while being consistent with external estimates of bigeye natural mortality. Besides, sensitivity optimization runs were done to test different mortality profiles and to attempt to estimate the mortality rates rather than the reproduction rates. Final calibrated parameters are shown in Table 2 and Figure 4 (panel Mortality), resulting in instantaneous rates between 0.026 mo^{-1} and 0.147 mo^{-1}. Including the variability with environmental conditions, the effective instantaneous mortality rates of juveniles vary between 0.6 and 1.1 y^{-1}, which is consistent with earlier estimates of 0.6-0.8 y^{-1} (Gaertner and Hallier, 2003) and 0.15-0.9 y^{-1} (Hampton, 2000) obtained from the tag attrition model.

The adult habitat index in SEAPODYM is defined as the function of accessible micronekton, with the accessibility function depending on oxygen tolerance and thermal preferences. Tagging data weren't used in the full likelihood in the yellowfin model. Rather, the model parameters for habitats and movement were initialized at values obtained in optimization with tagging data done in the tag movement model of SEAPODYM (see Senina et al., 2015). The parameters of thermal preferences estimated in the yellowfin CL model resulted in much wider range of temperatures to the T model, which estimated preferred temperature range 22-27°C throughout yellowfin lifespan. Besides, the CL model estimated linear relationship to the weight rather than to the species length, resulting in a very high temperature for juvenile habitat, above 30°C for youngest age classes, and a rapid decline to 13.5°C between 2 and 4 years old, which almost does not change for older ages (Figure 4, panel Adult habitat). For bigeye tuna, the habitat parameters are estimated in the CLT model, resulting in the temperature range between 25°C targeted by the recruits and 10°C by the oldest tunas, with age classes with mean lengths 85-155cm inhabiting waters 12-18°C (Figure 4, panel Adult habitat).

The movement parameters determine the diffusion and advection rates, which describe the velocities of non-directional and directional movement of population density. The yellowfin model is characterized by lower advection and higher diffusion than the bigeye model, which is typical for the CL model (Figure 4, panel Movement rates). The role of these parameter estimates in the overall movement pattern of yellowfin and bigeye tuna will be further discussed in Section 3.

2.3 Validation

Model validation is shown for the fit to the data, including the training and independent dataset. The fit to the catch data is quantified with help of three statistical scores: squared Pearson correlation coefficient between predictions and observations, standard deviation ratio and the normalized mean squared error. They are computed by fishery and for the total catch (Figure 6). The fit to the total catch is also shown as the time series in Figure 7, illustrating the small systematic underestimation of total catch in both models (small positive mean residual error) but rather small standard deviation of the standardized residuals and the absence of persistent bias (zero trend in residuals). Note that the fit remains similar for the validation sub-sets, which is 1979-1985 for yellowfin and 1998-2002 and 2017-2019 for the bigeye tuna model. It should be reminded here that the primary production derived from the PISCES model does not allow obtaining the good fit for the yellowfin catch data, mainly for the EPO purse-seine fleet associated with dolphins contributing almost 30% of the total yellowfin catches. The use of satellite-based primary production to simulate the micronekton density in the EPO improves the fit for associated PS fishery through a better habitat modelling. Note also, that the overall fit to the catch data was significantly improved in the bigeye model compared to the previous reference (Senina et al., 2021, Figure 9), with previous metrics (0.64,0.71,0.6) becoming (0.75,0.71,0.5).

The fit to the yellowfin length frequency data can be seen in (Senina et al., 2018, Figure C2). In the bigeye tuna model, the fit to the longline data was improved compared to the previous reference model (Senina et al., 2021, Figure A11), hence the comparison of predicted and observed length distributions is reported in this paper (Figure 8). It should be noted however, that there are still significant discrepancies for the length compositions of most purse-seine fisheries, mainly the overestimation of the large tuna proportions in the WCPO purse-seine fleets. The role of the EPO growth model in this misfit needs to be investigated further.

Finally, the fit to the tagging data, including the validation dataset, is shown in Figure 9. Unfortunately, tagging data validation still shows the deterioration of fit when including the 2000-2007 dataset, mainly due to the misfit east of

100W, where a vast number of modelled bigeyes have been moved, but were caught mostly either in the same area or to the west after being released at 95W.

2.4 Spatial structures

Estimating parameters from respective observational datasets, SEAPODYM suggests very different spatial structure of yellowfin and bigeye populations. First, the differences in the spawning habitat parameter estimates (Table 1, Figures 4-5) pointed out above, lead to the alternative, mutually exclusive spatial distributions of these species at early life stages. Figure 10 (top panel) shows that yellowfin larvae extend within the zone with the lowest concentrations of bigeye larvae. In other words, the study suggests that yellowfin and bigeye do not share the same habitat for spawning. The same can be said about the juvenile stock (young, immature stage) shown in Figure 10 (middle panel). During the pre-assessment workshop, it was noted that while the spatial distribution of juveniles predicted for yellowfin is consistent with the surface fisheries location and spatial extension, the same cannot be said for bigeye, whose juveniles are predicted to be outside of the fishing area. The spatial structure of juvenile bigeye is characterized by high densities between 10N-30N in the northern hemisphere and 5S-30S in the southern hemisphere, and the major hotspot in the central tropical ocean between 180E and 110W and 5S-20S. Note that predicted low densities of juvenile bigeye are still sufficient to sustain the fishing pressure in the tropical Pacific. Indeed, such spatial structure is driven by the CPUE data of various longline and surface fisheries (see Appendix B). Namely, these are the longline fleets, either targeting bigeye or albacore, which inform the model about high densities of juvenile bigeye in the sub-tropical zones (see ages 20-29 months in Figure B1a-d). The pole-and-line gear, although catching bigeye incidentally, shows the high abundance indices south-west of Kuroshio extension (Figure B2d). The high abundance indices for juvenile bigeye in the central tropical Pacific can be seen in the CPUE data of the Pacific Islands longline fleets (Figure B1c,d) and the CPUE of the surface gear fisheries (Figure B2). The latter informs the model about the eastward gradient, i.e., an increase of abundance indices towards the central Pacific Ocean, and highest abundance indices in the EPO (B2a-c). However, the high abundance is expected in the north of the equator as well, while the spatial distribution of juvenile (young) bigeye in Figure 10 fails to reproduce this, which is also confirmed by the poor statistical score for fishery S17 (EPO FAD fishery, see Figure 6b).

The spatial distributions of adult stages of yellowfin and bigeye tuna overlap in the tropical ocean, with the yellowin density predicted to be 2-3 times higher than that of bigeye in the tropical WCPO, and about the same in the equatorial EPO. To the south of 5S of the tropical Eastern Pacific, adult bigeye tuna is predicted to be more abundant than adult yellowfin tuna. The major differences between the two species spatial structures can be noted in the sub-tropical regions. Thus, the spatial distribution of yellowfin seems to be confined in the 20S-20N band, with the presence of yellowfin in the warm current systems of the western Pacific Ocean. Bigeye distribution extends much farther to the areas of temperate waters. Further, as the presence of bigeye in the 30-40N is consistent with catches and high CPUEs in these latitudes, similar predictions are made in the Southern Ocean, in particular the extension of the biomass along the East Australian current and south of the subtropical gyre whereas there are very few observations in this area.

Overall, the spatial structures of yellowfin and bigeye tuna populations through their respective life stages suggest the existence of a single tropical stock of yellowfin that depends on the recruitment across the equatorial Pacific Ocean, and three sub-stocks of bigeye, each of which relying on the recruitments in the central and eastern equatorial Pacific and on the edges of tropical zone of the ocean.

2.5 Stock and fishery impact estimations

The estimation of the model parameters by fitting the observed and predicted catch and length at fine spatial and monthly temporal resolutions implies that the model's spatial and age distributions of population density allow it to reproduce the spatial patterns of the observed abundance indices consistently with their size compositions. The stock estimation in SEAPODYM is done through finding the spatial distributions of biomass that simultaneously satisfy the following conditions: I) allows a good fit to all datasets, ii) sustains the fishing pressure through space, time and age, and iii) have minimal unobserved biomass (methods described in Senina et al., 2020a and SEAPODYM Reference Manual, 2022). Given the estimated age and spatial structures, the juvenile stocks of yellowfin and bigeye are nearly the same Pacific-wide, about 1Mt (million metric tonnes, see Figure 11) over the same time period, with WCPO accounting for about 80% of the yellowfin juvenile stock and 65% of the bigeye juvenile stock (Figure 12). The Pacific Ocean adult stocks of yellowfin is estimated at 4.9Mt and bigeye at 3.4Mt by the end of 2010. In the WCPO area, these figures are 2.37Mt for yellowfin and 1.35Mt for bigeye, remaining at the same level, 1.37Mt, at the end of 2019 (Figure 12, Adults).

For the WCPO area, the impacts of fishing expressed as the biomass ratio B_{Fref}/B_{F0} are 0.89 and 0.88 for recruits, 0.71 and 0.75 for juveniles, and 0.5 and 0.59 for adult stock of yellowfin and bigeye tuna respectively. The spatial maps of fishery impacts ($1-B_{fref}/B_{F0}$) on juvenile and adult stocks can be seen in Figure 11. Thus, locally in the WCPO area the depletion due to fishing (by the end of respective model simulation time) reaches 50% for juvenile yellowfin and 60% for juvenile bigeye, while the patterns is reversed for adult stocks, i.e., 70% maximal depletion for adult yellowfin and 50% for adult bigeye.

Comparison of the tuna stocks with the stock assessment model estimates (Vincent et al., 2020; Ducharme-Barth et al., 2020) show that in the overall WCPO area they are different, although SEAPODYM and MULTIFAN-CL agree on the estimation of the yellowfin adult stock and bigeye juvenile stock. Regionally, the discrepancies in the estimates of the juvenile yellowfin biomass come from regions 1-3 and 5-7, where the SEAPODYM biomass is estimated to be substantially lower. For bigeye, the discrepancies in the estimates of the adult biomass mainly come from regions 1, 5 and 6, where the SEAPODYM biomass is estimated to be substantially (4-5 times) higher than the biomass estimated by MULTIFAN-CL.

3. Regional connectivity

The movement probabilities were computed for the 9 Multifan-CL regions of "10N structure" (Vincent et al., 2020, Ducharme-Barth et al., 2020) and provided to the respective stock assessments as alternative models for movement. Note that the connectivity analyses were done for the populations in the absence of fishing. The regional movements are shown in Figures 13-21, excluding the pairs of regions for which all movement probabilities are below 0.05.

Region 1. The rates of emigration from the north-west Pacific region 1 are characterized by similar patterns throughout the ages but a lower residency for yellowfin than bigeye tuna. About 15-25% of juvenile yellowfin moves every quarter from this region to the warm pool regions 7 and 3, and 20-25% of adults leave this region, with the prevailing movement to the central Pacific region 2, then to a lesser extent to the tropical regions 3 and 7 (see also the paragraph on region 7 below). Note, the rates of immigration to region 1 are highest from region 2 for the early life stages of both species (Figure 14). The bigeye model shows 80-90% residency in region 1, with highest residency for the early life stages, and migration of adults to region 2 and 3 increasing with age up to 8% and 7% respectively, and to region 7 at levels of 5-6% per quarter. With respect to region 3, the model predicts immigration to region 1 with

probability 0.1 (Figure 15). This indicates the existing, although low, connectivity between tropical and sub-tropical sub-stocks of the bigeye tuna population.

In **Region 2**, the yellowfin model also shows lower residency, 60-82%, than the bigeye model, 82-90%, except for the ages of 6 years and older, when the residency levels are similar (Figure 14). For yellowfin, this region is mainly connected with region 4, where 10-25% of tunas aged 0-5 years move each quarter. However, considering the higher yellowfin biomass in region 4 and movement probabilities from region 4 to region 2 (Figure 16, Yellowfin), the net movement is positive for region 2 (from R4 to R2) for all life stages. For the bigeye tuna, the connectivity of regions 2 with regions 1 and 4 is similar among adults but showing greater seasonal variability between regions 2 and 4 (Figures 14 and 16, Bigeye).

Region 3 is the most inter-connected region, with 50-70% residency level for yellowfin and 50-65% for the bigeye tuna, and highest connectivity with regions 1, 4 and 8 (Figure 15). However, the movement patterns from region 3 to other regions are very different for yellowfin and bigeye tuna across the age dimension. For example, the highest rates of emigration to region 4 decrease with age for juvenile yellowfin and increase for adult, with the inflection point coinciding with the age at maturity (20.5 months, Figure 3), but it increases for bigeye at early life stages, up to 20% in the second quarter, and then decreases across the age (see Figure 15, Bigeye). Note that given the movement rates and regional biomass, the net movement of bigeye tuna is directed from region 3 to region 4 for juveniles and adult bigeye, with highest rates at juvenile stage. For yellowfin, the net movement between regions 3 and 4 is zero for larvae and juvenile stages, and positive (from R3 to R4) only for adult stages.

Region 4. For both tuna species, the central tropical region 4 has higher residency that region 3, with levels 80% for early life stages of yellowfin and bigeye, which reduce with age to 60-70% (yellowfin) and 70% (bigeye). For both tuna, region 4 is the recipient of the larval biomass from the EPO, which is presumably transported by the north equatorial current. Further movement of bigeye larvae from region 4 to region 3 also exists, but direction of net movement is highly variable seasonally (Figures 15-16, Bigeye) and inter-annually. For juvenile life stages, the models predict the opposite pattern, i.e., the net movement of juvenile yellowfin from the EPO to region 4, and the net movement of juvenile bigeye from the central Pacific to the EPO. For adult life stages of both tunas, region 4 is the recipient of the biomass from region 3 (Figure 15), and the donor region for the EPO (Figure 16). Also, for both species, tropical stock in region 4 is mixing with regions 2 and 6, however the net movements between these regions are either close to zero or variable seasonally.

Region 5. The residency of yellowfin tuna in region 5 is predicted to vary at levels 60-80%, with highest residency at early life stages. The bigeye tuna model predicts for this region almost 90% residency at early life stages, slowly reduced to 73% though age. Both tunas' juveniles are predicted to move actively between region 5 and 8 (Figures 17 and 20, Yellowfin), with the net movements being positive for region 8 (From R5 to R8). Adult yellowfin is moving from this region to region 6. The movement in the opposite direction is weaker for yellowfin (Figure 18, Yellowfin). For adult bigeye, the model shows a substantial mixing between region 5 and 6 (Figures 17-18, Bigeye). Given the species spatial structure and additional connectivity analysis conducted with regions 5 and 6 split latitudinally, the model shows that the westward movement occurs between 10S and 23.5S, and the eastward movement in the sub-tropical part of regions 5 and 6.

In **Region 6**, the residency of yellowfin is predicted to vary at levels 60-80%, with lowest residency for 1-1.5 years old juveniles, which are migrating to the tropical region 4 (Figure 18, Yellowfin). Bigeye tuna residency here is predicted to be very high for early life stages, 95%, reducing to 80% by the age at maturity and then stabilizing at 78% for oldest

tunas (Figure 18, Bigeye). Predicting high densities of juvenile bigeye in the tropical part of region 6, the model shows their net movement from region 6 to regions 4 and 5.

Region 7 is connected with regions 1 and 3, although both models predict high residency of tuna species in this region, 83-97% for yellowfin and 87-92% for bigeye. Note, due to the coarse resolutions of reference models, the model predictions in region 7 account only the part of the Pacific Ocean and the Philippine Sea (see Figure 10). As pointed above, there is mainly the immigration to region 7 from region 1 of both tunas at all life stages. The exception is the adult yellowfin, for which region 7 is a donor to region 1.

Region 8 includes the Bismarck and the Solomon Seas, known as hotspots for tunas. The reference yellowfin model predicts the maximal densities of yellowfin larvae, and both models show significant abundances of juveniles and adults in this region (Figure 10). The model predicted residency is low for both species, 30-65% for yellowfin and 28-75% for bigeye, decreasing with age (Figure 20). The region is connected with regions 3 (highest emigration rates), 5 (medium rates) and 7 (low rates). For yellowfin larvae, the connectivity analysis shows the net movements from region 8 to adjacent regions, while for bigeye larvae, they are predicted to be transported here from regions 3 and 5. For juvenile stages, the yellowfin movements are variable, and the juveniles of bigeye migrate from region 5 to region 8 and from region 8 to region 3 and, to a lesser extent, to region 7. The net movements of adults, both yellowfin and bigeye, are predicted to move from region 8 to region 3.

Region 9 is a small 5x10° region, which is included in the stock assessment model based on high tag recapture rates indicating the tuna residency in this area. On the contrary, the SEAPODYM models show low residency for this region. Such discrepancy could be explained if the observed high recapture rates were due to the seasonal migrations of tunas, however the current coarse resolution models cannot be used to verify this hypothesis given their inability to represent the dynamics of a fine-scale coastal current system, characterized by seasonal upwelling and high productivity (Brinkman et al., 2001).

Overall, the reference models show the evolution of tuna movement and hence the regional connectivity across the age dimension. This is the emerging property of the SEAPODYM models, which is driven by the change of thermal preferences with increasing size of individuals, and consequently the extension of both vertical and horizontal habitats while tunas become bigger. That is why in most cases, the residency decreases with age. Note also, that the lower residency of yellowfin tuna compared to that of bigeye tuna is likely associated with the prevailing non-directional (diffusive) movement estimated in the yellowfin reference model. These results will be re-visited once the model is updated with the tagging data in the full likelihood context.

Another emergent property is the change of movement pattern occurring around the age at maturity (20.5 months for yellowfin and 36.5 months for bigeye). In particular, this is well seen in the movement rates within the tropical regions 3, 4, 7-9. Considering that the assumption of opportunistic spawning made in the reference models implies that the successful spawning occurs where the spawning and feeding habitats overlap, there is no specific mechanism in the model which alters the behavior of tunas once they reach maturity. Therefore, such abrupt change in tuna movement before or after the specified age at maturity can only be driven by data.

Acknowledgments

We thank Peter Williams for timely provisions and updates of the geo-referenced fisheries data, and Sylvain Caillot for providing the conventional tagging data.

4. References

Brinkman, R., Wolanski, E., Deleersnijder, E., McAllister, F., Skirving, W. 2001. Oceanic inflow from the Coral Sea into the Great Barrier Reef. Estuarine, Coastal and Shelf Science, 54, 655–668. doi:10.1006/ecss.2001.0850

Ducharme-Barth, N., Vincent, M., Hampton, J., Hamer, P., Williams, P., Pilling. G. 2020. Stock assessment of bigeye tuna in the western and central Pacific Ocean. Western and Central Pacific Fisheries Commission Scientific Committee, Working Paper. WCPFC-SC16-2020/SA-WP-03.

Farley, J., Eveson, P. Krusic-Golub, K., Sanchez, C., Roupsard, F., McKechnie, S., Nicol, S., Leroy. B., Smith, N, Chang, S-K. Project 35: Age, growth and maturity of bigeye tuna in the western and central Pacific Ocean. WCPFC-SC13-2017/SA-WP-01, Scientific Committee thirteenth regular session, Rarotonga, Cook Islands, 9 – 17 August 2017.

Gaertner, D, Hallier, J.-P. 2003. Estimate of natural mortality of bigeye tuna (Thunnus obesus) in the Eastern Atlantic from a tag attrition model. Col. Vol. Sci. Pap. ICCAT, 55(5): 1868-1879.

Hampton, J. (2000). Natural mortality rates in tropical tunas: size really does matter. Canadian Journal of Fisheries and Aquatic Science, 57:1002–1010.

Hampton, J., Langley, A., Kleiber, P. 2006. Stock assessment of yellowfin tuna in the western and central Pacific Ocean, including an analysis of management options. WCPFC SC2 SA WP-1. Manila, Philippines, 7-18 August 2006.

Harley, S. J., Davies, N., Hampton, J., and McKechnie, S. (2014). Stock assessment of bigeye tuna in the Western and Central Pacific Ocean. Technical Report WCPFC-SC10-2014/SA-WP-01, Majuro, Republic of the Marshall Islands, 6–14 August 2014.

Langley, A., Hoyle, S., Hampton, J. 2011. Stock assessment of yellowfin tuna in the Western and Central Pacific Ocean. Western and Central Pacific Fisheries Commission Scientific Committee, Working Paper. WCPFC-SC7-2011/SA- WP-03.

Lehodey, P. and B. Leroy. 1999. Age and growth of yellowfin tuna (Thunnus albacares) from the western and central Pacific Ocean as indicated by daily growth increments and tagging data. WP YFT-2, SCTB 12, Papeete, French Polynesia, 16 ?23 June 1999.

Lehodey P. et al. 2017. Modelling the impact of climate change including ocean acidification on Pacific yellowfin tuna. Western and Central Pacific Fisheries Commission Scientific Committee, Working Paper WCPFC- SC13-2017/EB-WP-01, 2017.

Nicol, S., Lehodey, P., Senina, I., Bromhead, D., Frommel, A.Y., Hampton, J., Havenhand J., Margulies D., Munday P. L., Scholey V., Williamson J. E., Smith N. 2022. Ocean Futures for the World's Largest Yellowfin Tuna Population Under the Combined Effects of Ocean Warming and Acidification. Front. Mar. Sci., 9. doi.org/10.3389/fmars.2022.816772

SEAPODYM: spatial ecosystem and population dynamics model for migratory age-structured stocks [version 4.0]. Reference Manual, Pacific Community, 186pp. https://purl.org/spc/digilib/doc/vxsz3

Senina, I., Lehodey, P., Calmettes, B., Nicol, S., Caillot, S., Hampton, J. and P. Williams. 2015. SEAPODYM application for yellow tuna in the Pacific Ocean. Western and Central Pacific Fisheries Commission Scientific Committee, Information Paper. WCPFC-SC11-2015/EB-IP-01.

Senina, I., Lehodey, P., Calmettes, B., Dessert, M., Hampton, J., Smith, N., Gorgues, T., Aumont, O., Lengaigne, M., Menkes, C., Nicol, S., Gehlen, M. 2018. Impact of climate change on tropical Pacific tuna and their fisheries in Pacific Islands waters and high seas areas. Western and Central Pacific Fisheries Commission Scientific Committee, Working Paper. WCPFC-SC14-2018/EB-WP-01

Senina, I., Lehodey, P., Sibert, J., Hampton, J., 2020a. Integrating tagging and fisheries data into a spatial population dynamics model to improve its predictive skills. Can. J. Fish. Aquat. Sci. doi:10.1139/cjfas-2018-0470.

Senina, I., Lehodey, P., Nicol, S., Scutt Phillips, J., Hampton, J. 2020b. SEAPODYM: revisiting bigeye reference model with conventional tagging data. Western and Central Pacific Fisheries Commission Scientific Committee, Information Paper. WCPFC-SC16-2020.

Senina, I., Briand, G., Lehodey, P., Nicol, S., Hampton, J., Williams, P. 2021. Reference model of bigeye tuna using SEAPODYM with catch, length and conventional tagging data. Western and Central Pacific Fisheries Commission Scientific Committee, Information Paper. WCPFC-SC17-2021/EB-IP-08.

Vincent, M., Ducharme-Barth, N., Hamer, P., Hampton, J., Williams, P., Pilling. G. 2020. Stock assessment of yellowfin tuna in the western and central Pacific Ocean. Western and Central Pacific Fisheries Commission Scientific Committee, Working Paper. WCPFC-SC16-2020/SA-WP-04.

List of Tables

Table 1: Sources of forcing variables and details of SEAPODYM model configurations used in simulations and parameter estimation (referring to the time period when data are augmented to the likelihood). Note that all variables were interpolated onto the SEAPODYM grid with the resolution shown under Spatiotemporal resolutions.

	Yellowfin model	**Bigeye model**
	Physical forcing	
T, u, v	NEMO global simulation with ERA-INTERIM atmospheric reanalysis, ORCA2 configuration, available for the 1979-2010 time period	NEMO global simulation with ERA5 atmospheric reanalysis, ORCA025 configuration, available for the 1993-2019 time period
	Biogeochemical forcing	
PP, Z	NEMO-PISCES coupled model simulation with ORCA2 configuration for the 1979-1997 time period and EPPLEY-VGPM primary production derived from satellite Chl-a for the 1998-2010 time period	EPPLEY-VGPM primary production and Morel's model euphotic depth derived from satellite Chl-a, available at $0.25° \times 7d$ resolution and starting in January 1998
$O2$	NEMO-PISCES coupled model simulation with ORCA2 configuration, available for the 1979-2010 time period	WOA climatology at $1/4° \times 30d$ and climatological year
	Biological forcing	
F	SEAPODYM-LMTL model global simulation on regular $1° \times 30d$ and $2° \times 30d$ resolutions and for the 1979-2010 time period with satellite-based primary production starting 1998 as forcing	SEAPODYM-LMTL model simulation on regular grid with $0.25° \times 7d$ resolution and for the 1998-2019 time period
	Spatiotemporal resolutions	
$\Delta\mathbf{x} \times \Delta t$	$1° \times 30d$, $2° \times 30d$	$2° \times 30d$
	Age resolution and structure	
n_a, Δa	60 age classes of size $30d$	84 age classes of size $30d$
$A+$	5 years	7 years
	Time periods	
simulation	1/1979 -12/2010	1/1998 -12/2019
likelihood	1/1986 -12/2010	1/2003 -12/2017

Table 2: SEAPODYM parameters. Parameters marked by asterisks were fixed in optimization experiment. Parameter with [or] were estimated at their lower or upper boundary respectively.

θ	**Description**	**YFT**	**BET**
	Reproduction		
σ_0	standard deviation in temperature Gaussian function at age 0, $°C$	1.85	3.31
$T_0^\star$	optimal surface temperature for larvae, $°C$	28.94	[25.5
α_P	prey encounter rate in Holling (type III) function, day^{-1}	0.78	[1e-4
α_F	Log-normal mean parameter predator-dependent function, g/m^2	0.21	[0.2
β_F	Log-normal shape parameter in predator-dependent function	0.91	2]
R	reproduction rate in Beverton-Holt function, mo^{-1}	[0.05	0.02
b	slope parameter in Beverton-Holt function, nb/km^2	10*	10.16
	Mortality		
$\bar{m}_p$	predation mortality rate age age 0, mo^{-1}	0.1*	0.15*
β_p	slope coefficient in predation mortality	0.18	0.04*
$\bar{m}_s$	senescence mortality rate at age 0, mo^{-1}	3e-04	1e-4*
β_s	slope coefficient in senescence mortality	1.16	1.13*
ϵ	variability of mortality rate with habitat index $M_H \in (\frac{M}{(1+\epsilon)}, M(1+\epsilon))$	2.07	0.1*
	Habitats		
T_0	optimal temperature (if Gaussian function), or temperature range for the first young cohort, $°C$	35.47	26.18
T_K	optimal temperature (if Gaussian function), or temperature range for the oldest adult cohort, $°C$	13.25	[10.0
b_T	allometric power coefficient for thermal preferences at age	3.0]	0.69*
γ	slope coefficient in the function of oxygen)	[1e-04	[1e-4
$\hat{O}$	threshold value of dissolved oxygen, ml/l	0.41	[0.7
eF_1	contribution of epipelagic forage to the habitat	0.37	1.5]
eF_1	contribution of mesopelagic forage to the habitat	[0.35	1.5]
eF_1	contribution of migrant mesopelagic forage to the habitat	[0.35	0*
eF_1	contribution of bathypelagic forage to the habitat	0*	0*
eF_1	contribution of migrant bathypelagic forage to the habitat	0*	[0
eF_1	contribution of highly migrant bathypelagic forage to the habitat	[0.35	1]
	Movement		
V_m	maximal sustainable speed of tuna in body length, BL/sec	[0.7	[0.15
a_V	slope coefficient in allometric function for maximal speed	[0.85	0.75*
σ	multiplier for the maximal diffusion rate	0.9*	1.2]
c	coefficient of diffusion variability with habitat index	0.3*	0.9*

List of Figures

a) Yellowfin tuna

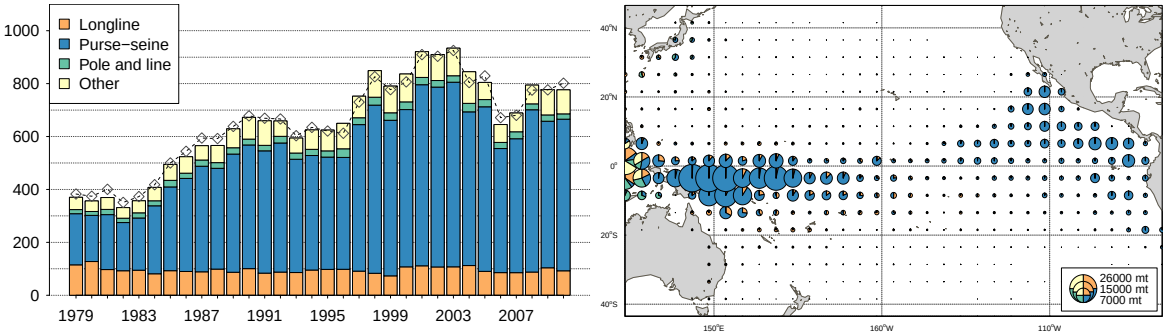

b) Bigeye tuna

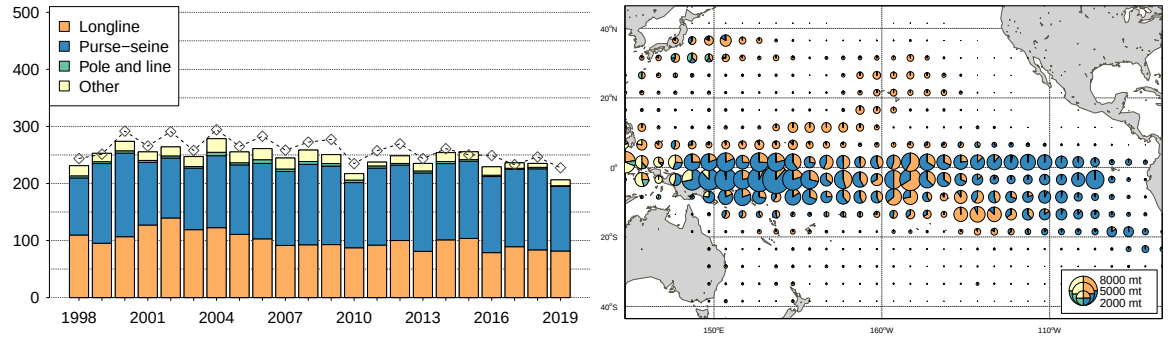

Figure 1: Total catch by gear of yellowfin and bigeye tuna aggregated from the georeferenced catch (Pacific-wide) that was used in SEAPODYM modelling. Dashed line corresponds to total landings data (SPC Yearbook, 2019).

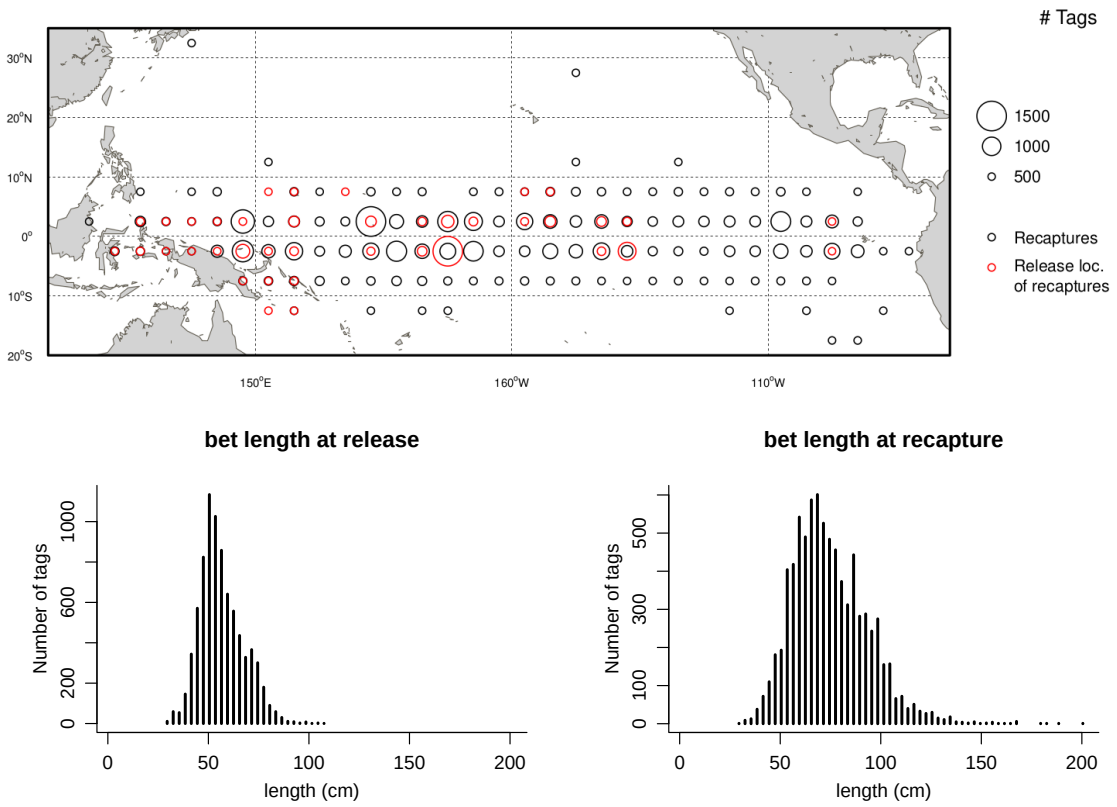

Figure 2: Top panel map: number of bigeye tuna tagged and recaptured during conventional tagging campaigns over the 2007-2014 time period that were used to inform SEAPODYM model parameters. Bottom panel: observed bigeye size distributions at release and recapture.

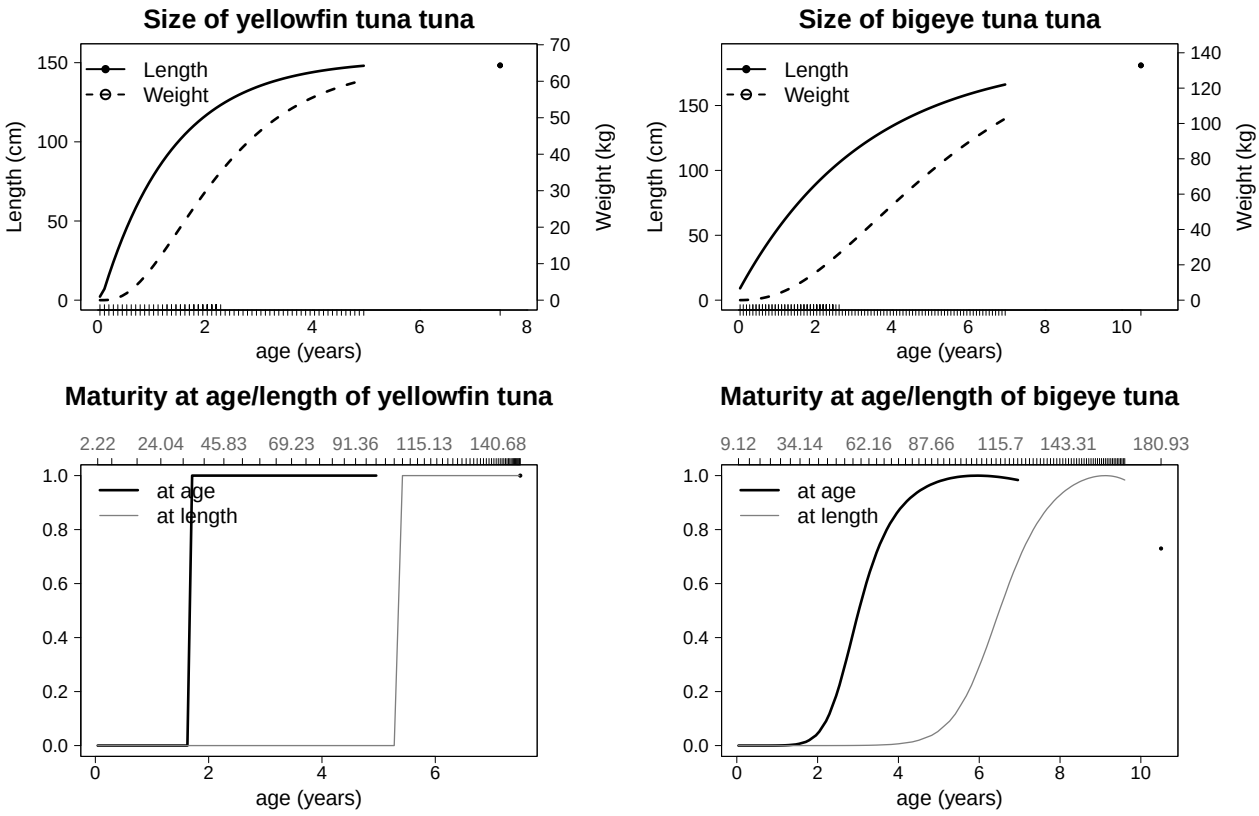

Figure 3: Static model parameters used in model configurations. Mean length and weight are interpolated from the Multifan-CL estimated functions (Langley et al., 2011; Harley et al., 2014) at the mid-point of each age class indicated with the outer tick marks of the x-axis. The inner ticks of the x-axis show the ages at which the habitat indices were evaluated in the current reference model. Maturity-at-age are estimated in Farley et al., 2014 (yellowfin) and Farley et al., 2017 (bigeye). Maturity-at-length is shown according to the growth model used in the SEAPODYM configurations.

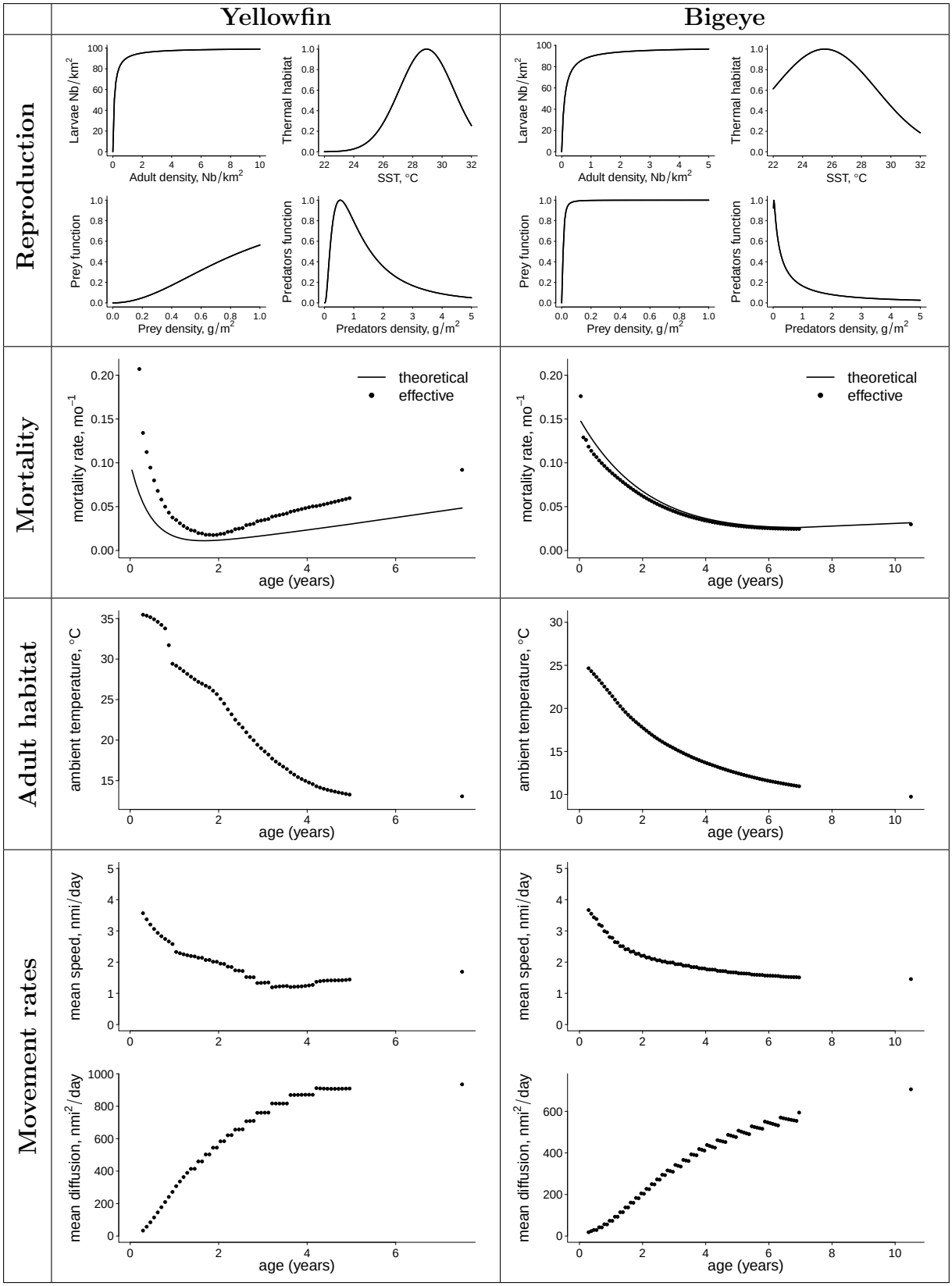

Figure 4: Estimated functional relationships in the main dynamic processes (reproduction, natural mortality and movement) of the reference MLE models. Habitat temperature and movement rates are computed as weighted spatio-temporal average with weights being the population density at age.

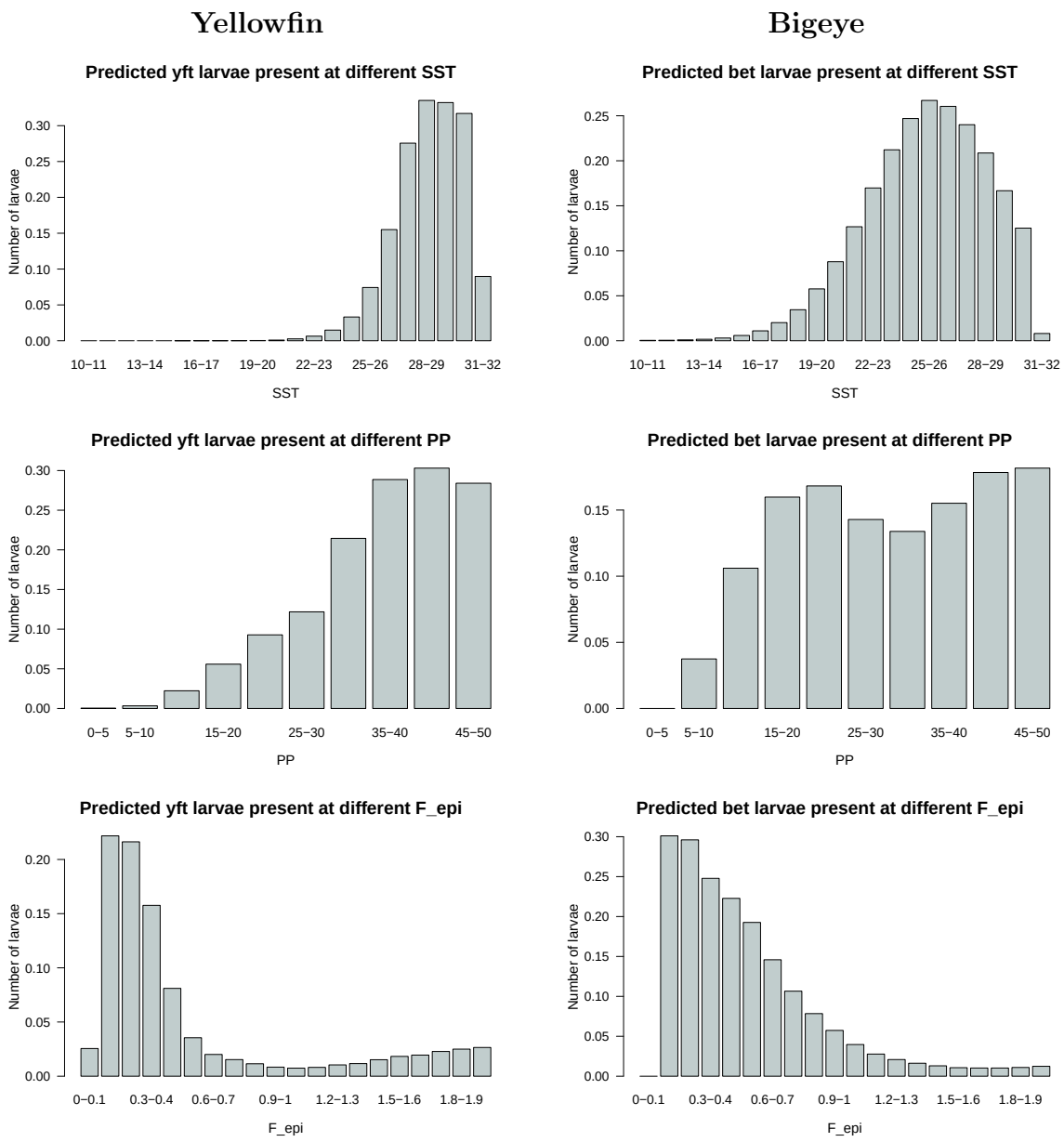

Figure 5: Predicted mean number of yellowfin (left) and bigeye (right) larvae in association with sea surface temperature, primary production and epipelagic forage.

a) Yellowfin **b) Bigeye**

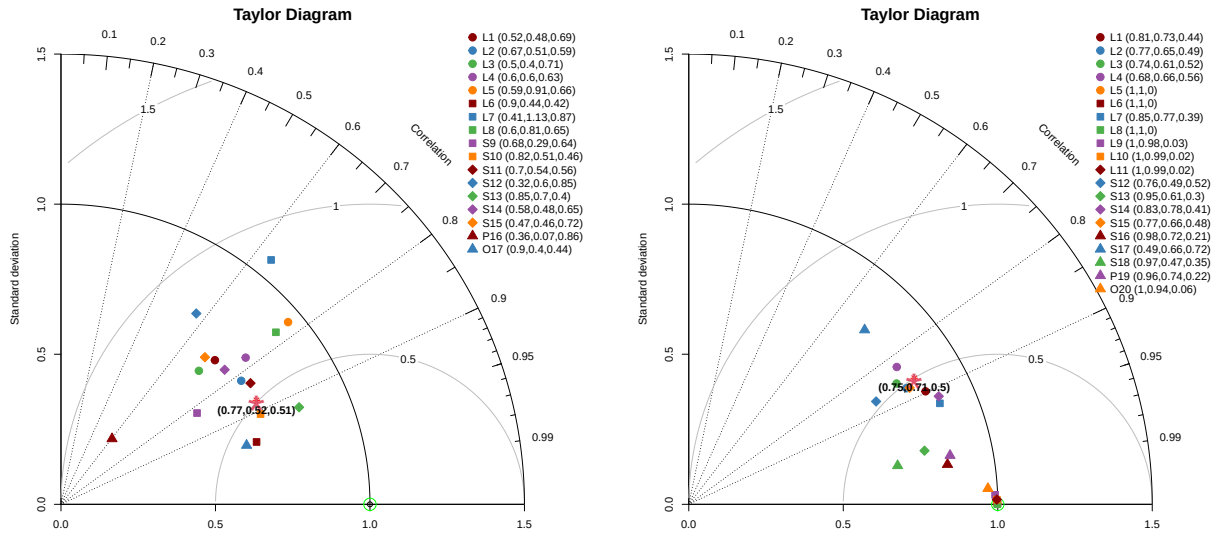

Figure 6: Model validation for the geo-referenced catch data with seven years of independent data included: Taylor diagrams show aggregated metrics of the model fit to the data: correlation (angular coordinates) between predictions and observations, standard deviation ratio (distance from (0,0)) and normalized mean squared error (concentric circles with the green bullet being the center). Each point on the graph shows three metrics of the fit to the catch data by fisheries (Table 1).

a) Yellowfin **b) Bigeye**

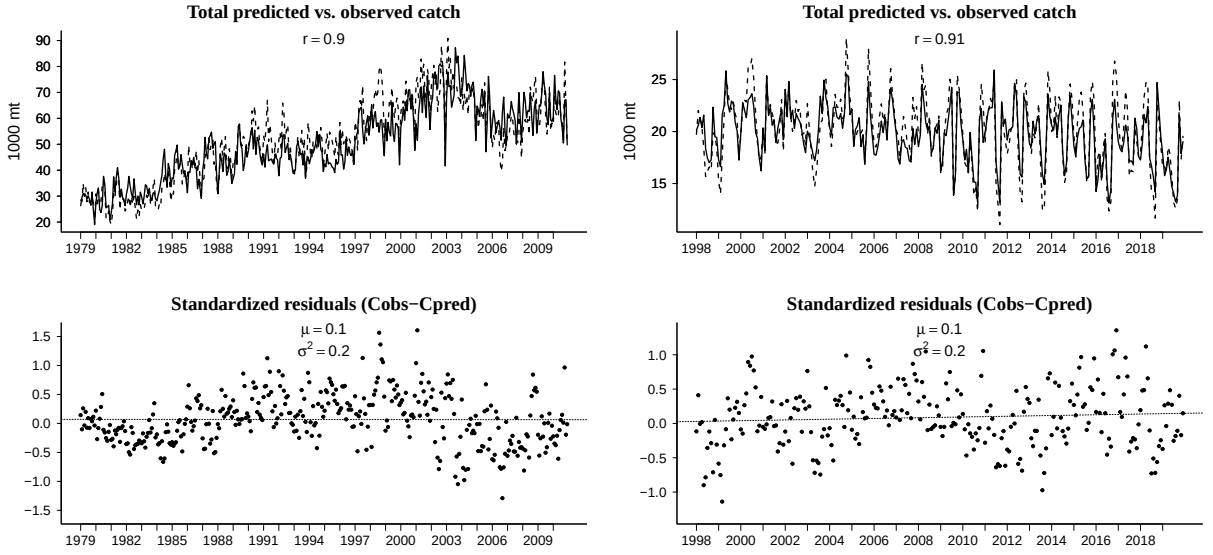

Figure 7: Observed vs. predicted monthly catch and residuals of catch of yellowfin (a) and bigeye (b) tuna. In the yellowfin model, the first 5 years of data were not included into the likelihood. In the bigeye model, the data before 2003 and after 2017 were not included into the likelihood.

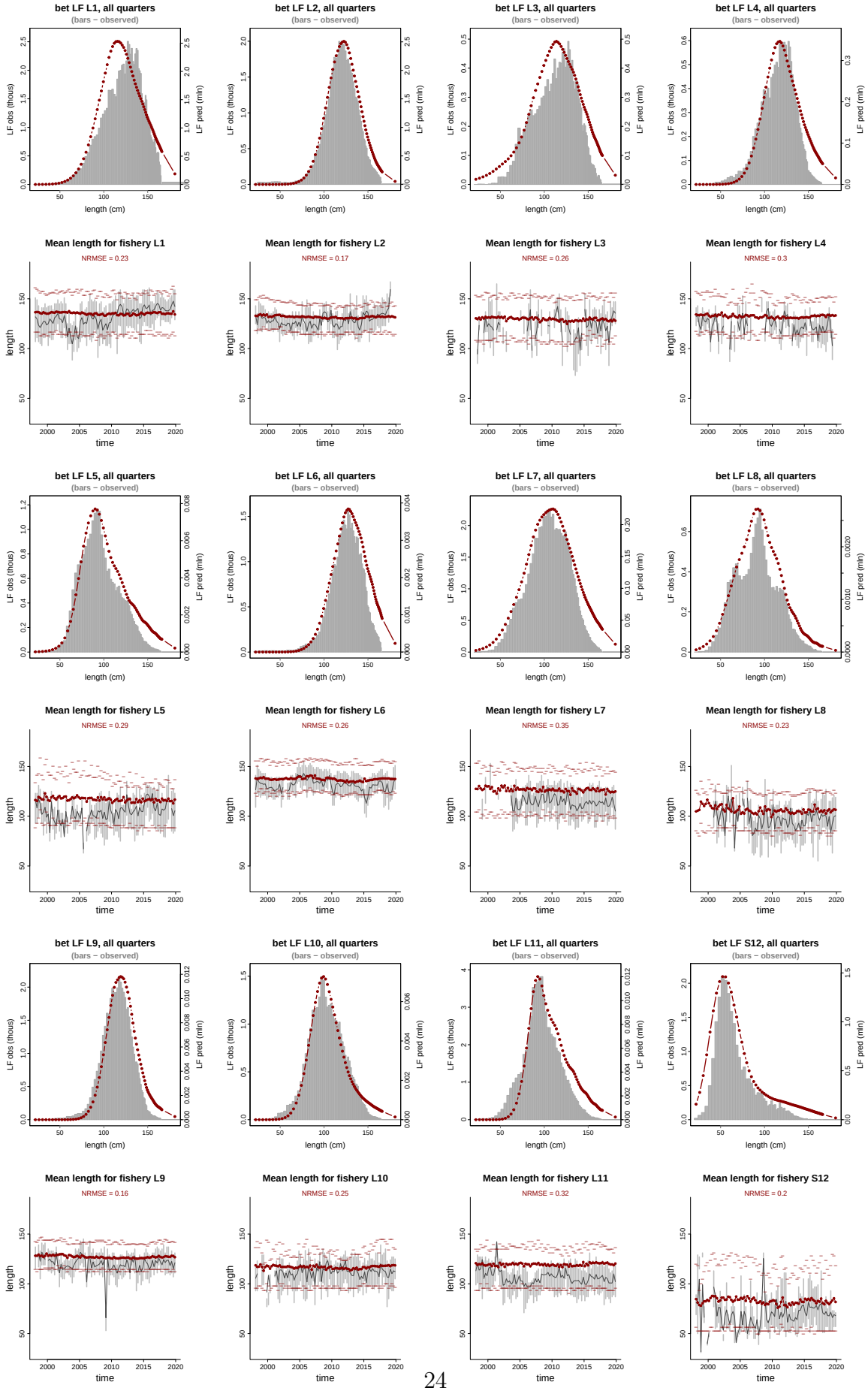

Figure 8: Observed (grey) and predicted (red) length frequencies distribution and mean length in catches of bigeye tuna.

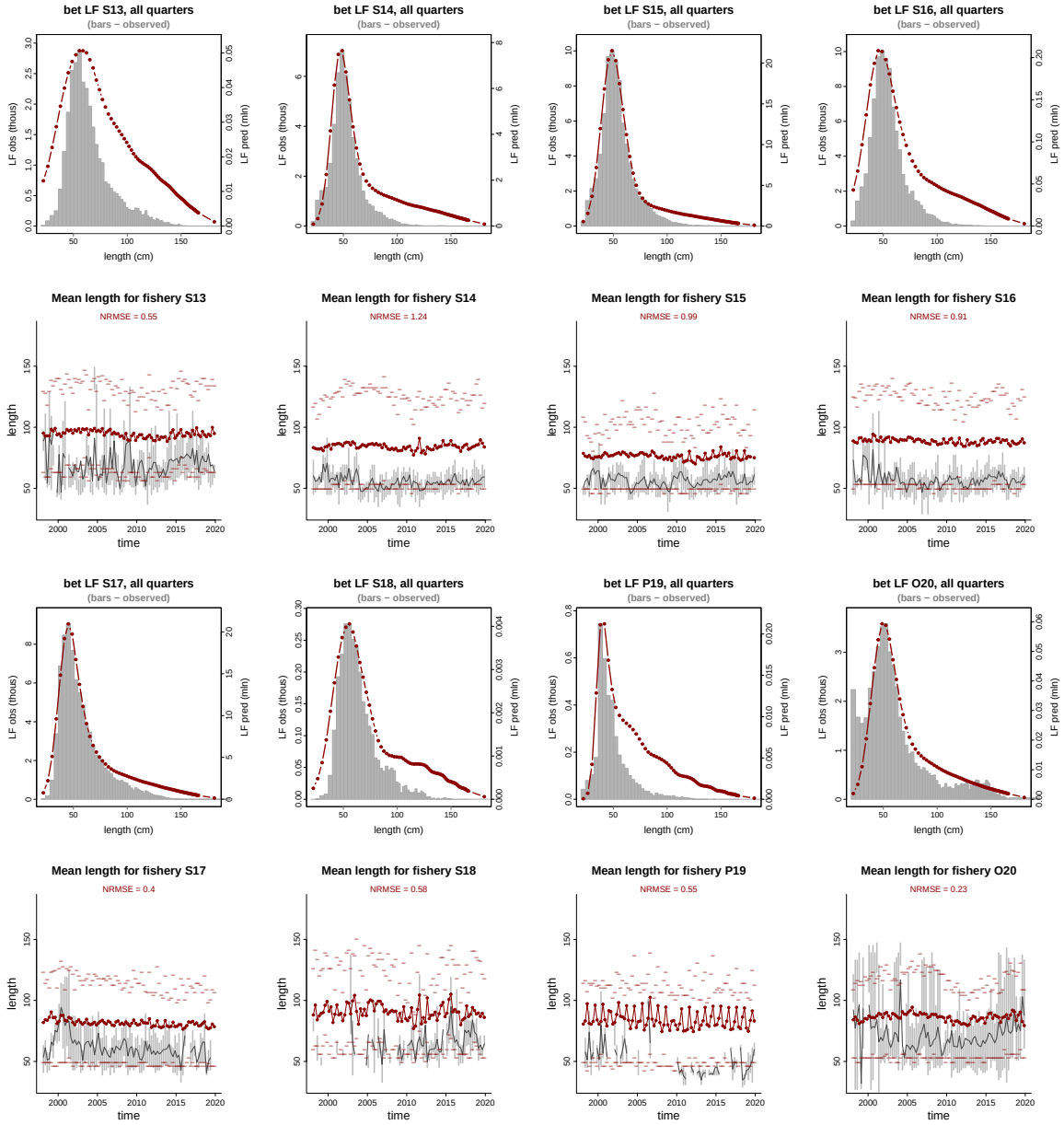

Figure 8: Fit for the length frequencies data. Continued.

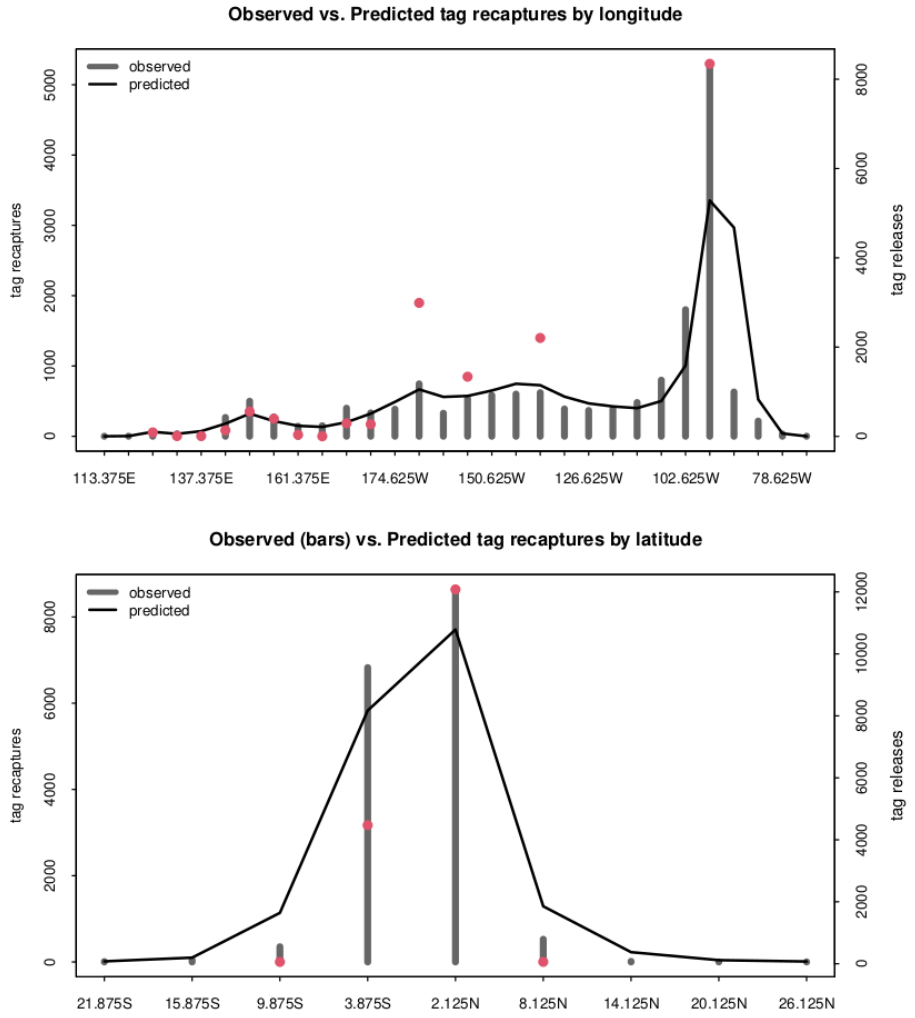

Figure 9: Tag recapture model validation: number of observed (bars) and predicted (lines) bigeye tuna recaptures between May 2000 and June 2014 shown as longitudinal and latitudinal profiles of tag recapture distributions. Distributions of tag recaptures were predicted with the MLE parameters estimated by the CLT model, which included the 2008-2014 sub-set of tagging data. Validation metrics for the optimization sub-set are (0.84,0.89,0.4) and for the entire dataset are (0.67,0.55,0.58). Releases (right y-axis) are added to these plots as red dots.

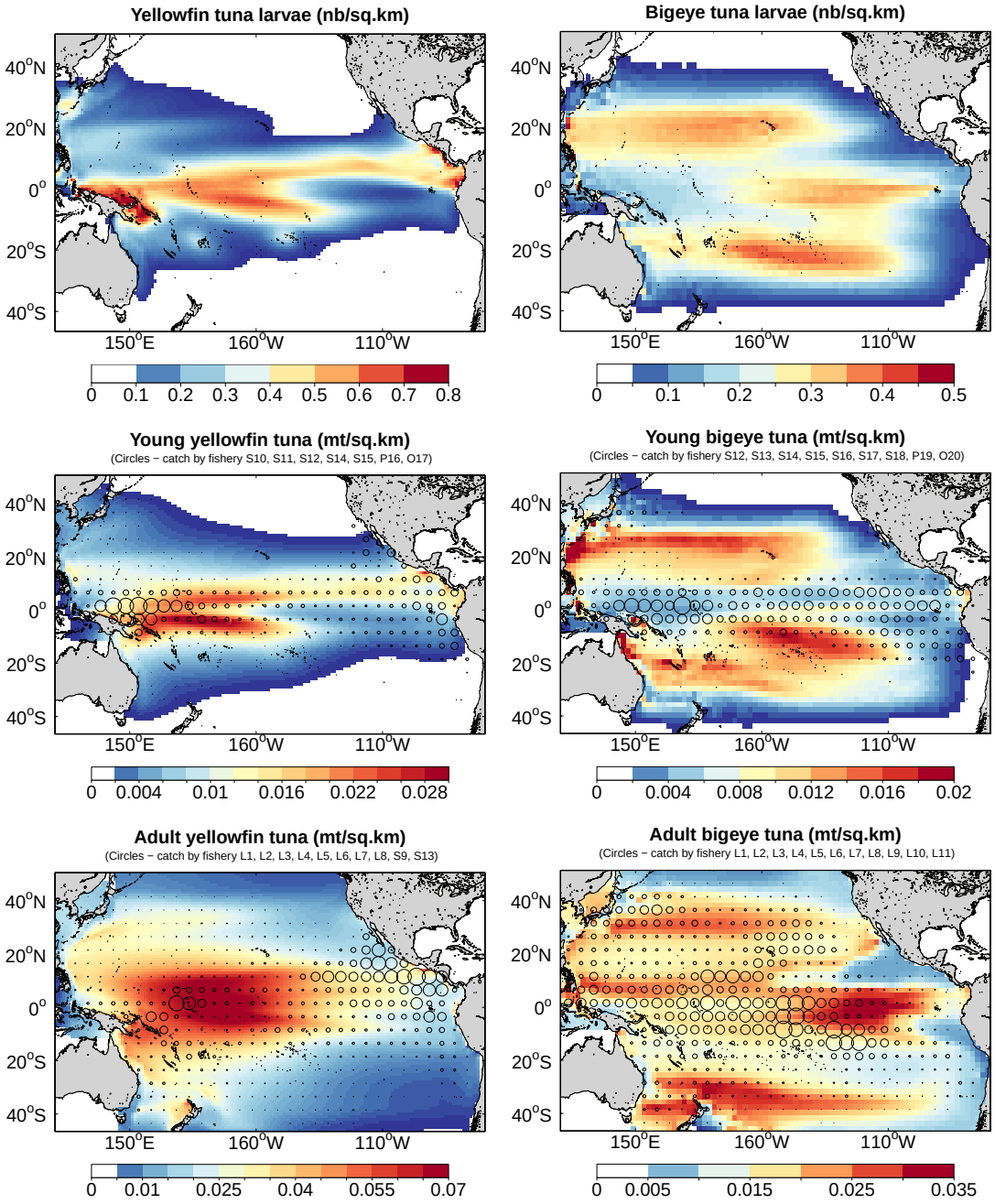

Figure 10: From top to bottom: average density of fished populations of yellowfin (left) and bigeye (right) tuna by life stage: larval (Nb/km^2), juvenile (mt/km^2, all age classes older than 3 months of age and younger than age at 50% maturity) and adult (mt/km^2, age classes older than age at 50% maturity) yellowfin and bigeye tuna.

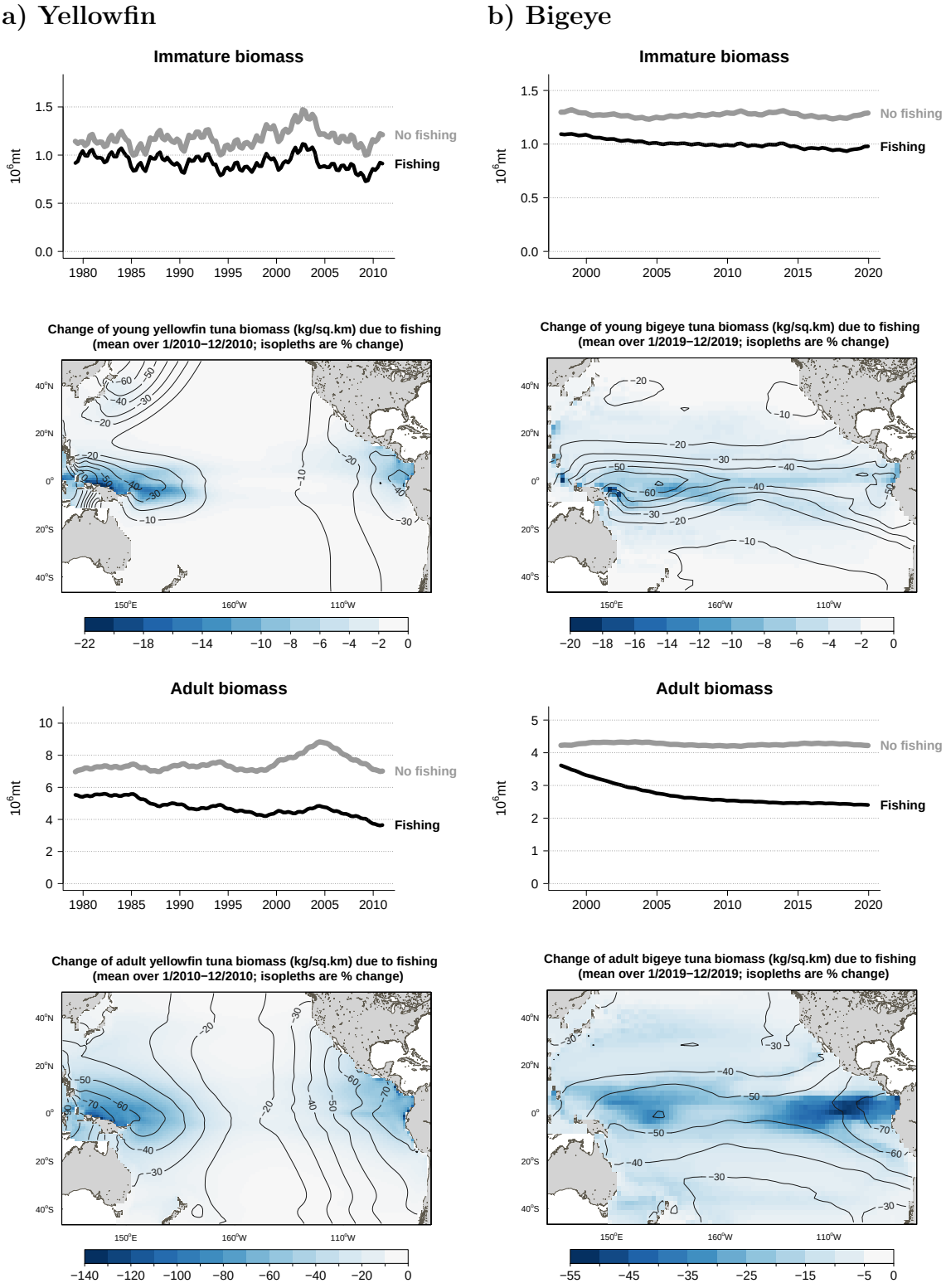

Figure 11: Spatial fishing impact on young and adult population stages of yellowfin and bigeye tuna. Contour lines show index $100 \cdot \frac{B_{ref} - B_{F0}}{B_{F0}}$ and colour shows the average biomass change $B_{ref} - B_{F0}$ due to fishing.

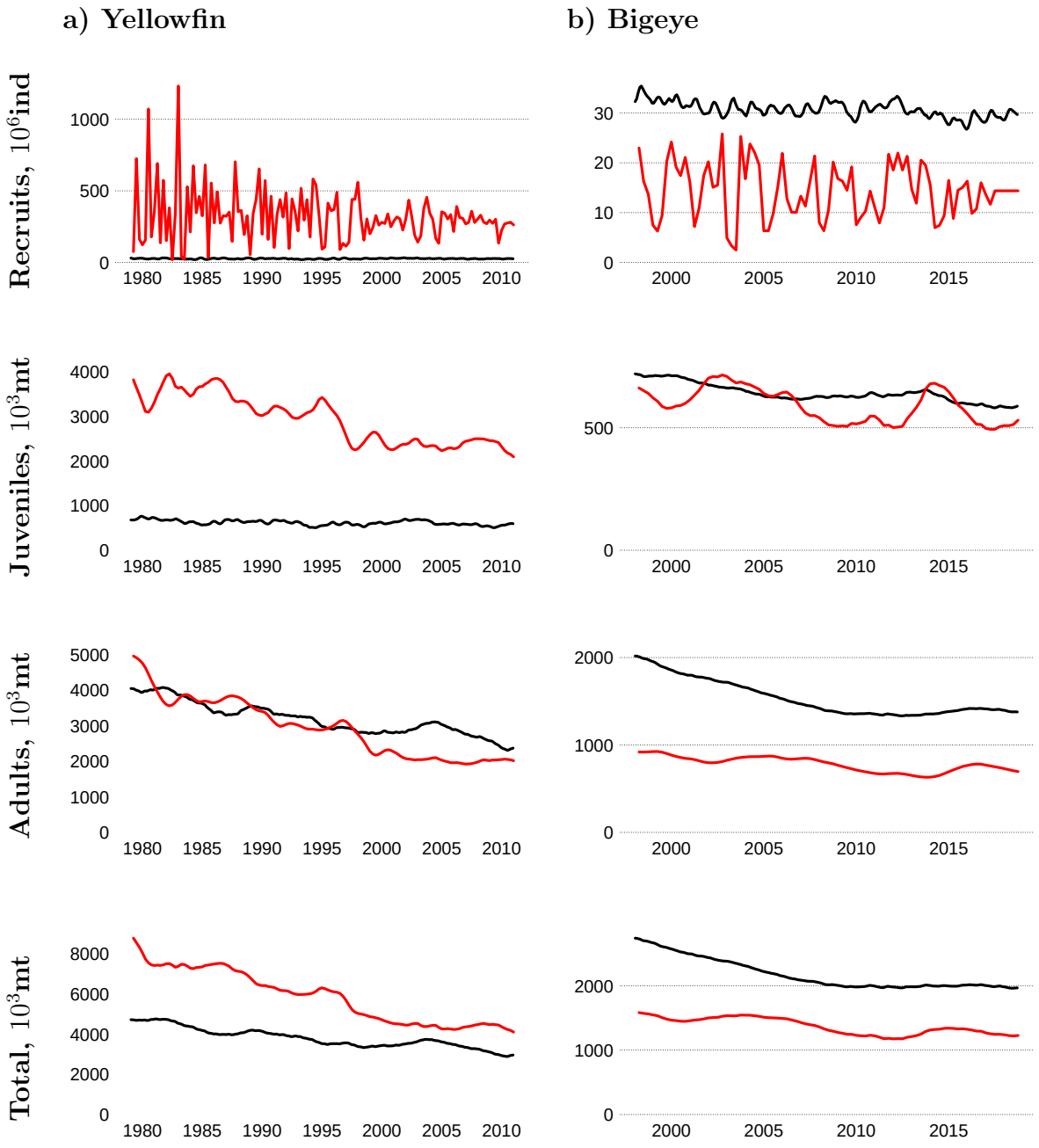

Figure 12: Comparison between regional SEAPODYM (black) and Multifan-CL (red) estimates of yellowfin (left) and bigeye (right) tuna population abundance of recruits, and the biomass of juveniles (aged older than 3 months and younger than the age at 50% maturity) and mature (50% maturity and older) life stages in the WCPO area. The Multifan-CL estimates are taken from previous assessments of yellowfin (Vincent et al., 2020) and bigeye (Ducharme-Barth et al., 2020) tuna stocks. Note, the unit of abundance is million individuals and the unit of biomass is thousand metric tons.

Region 1. Yellowfin

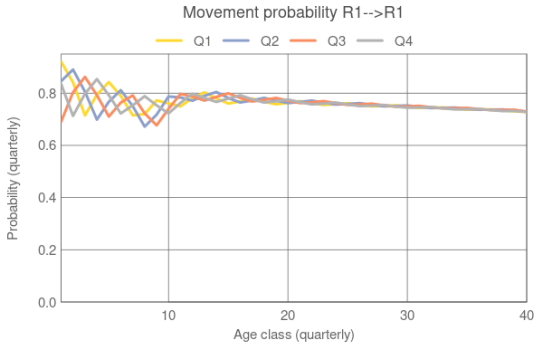

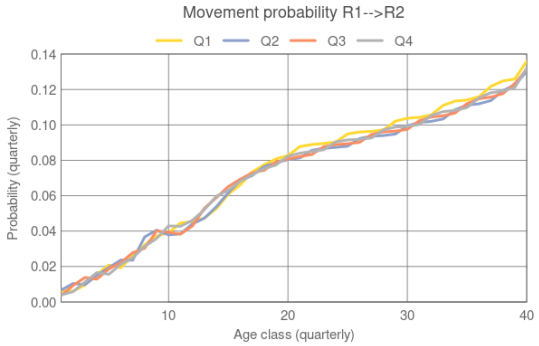

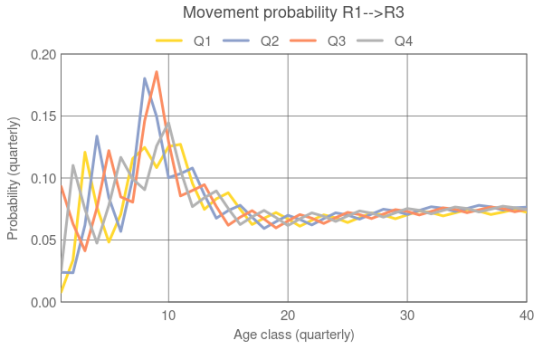

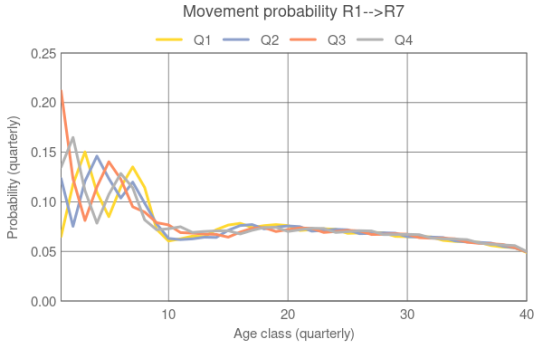

Region 1. Bigeye

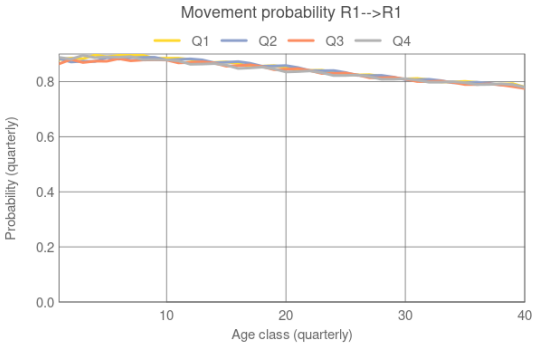

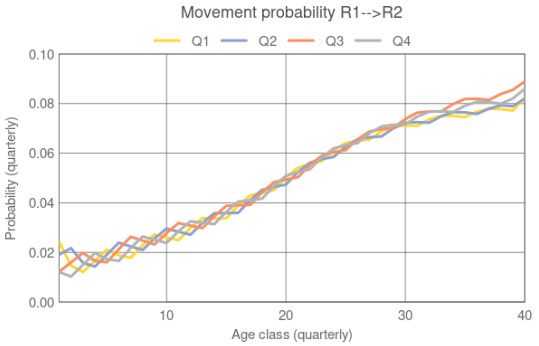

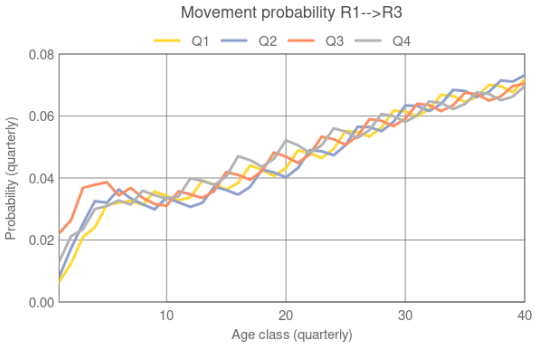

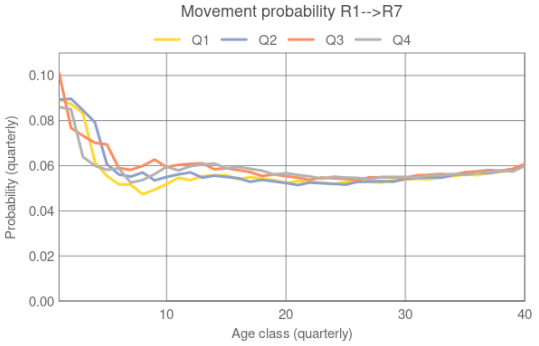

Figure 13: Regional movement probabilities from region 1 derived from SEAPODYM for the 9 Multifan-CL regions of "10N structure" (Vincent et al., 2020, Ducharme-Barth et al., 2020). Note, regions with all movement probabilities below 0.05 are not shown.

Region 2. Yellowfin

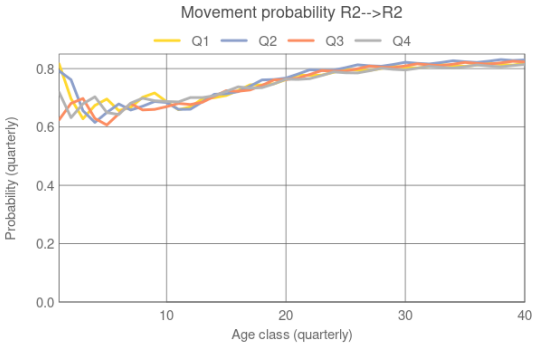

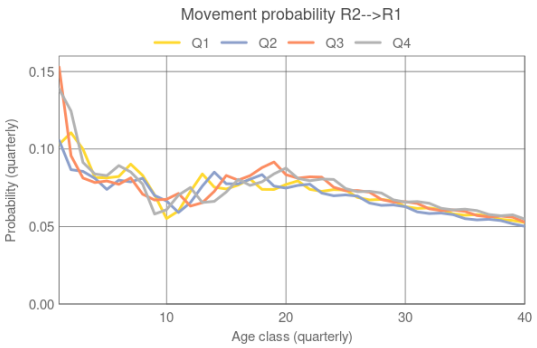

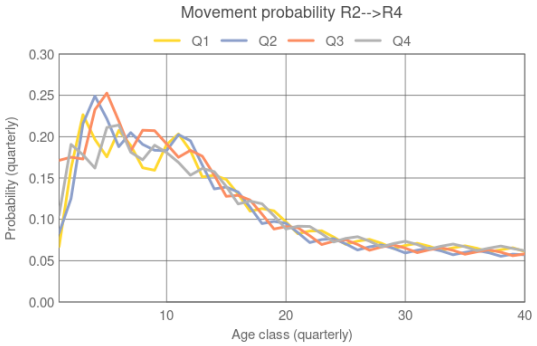

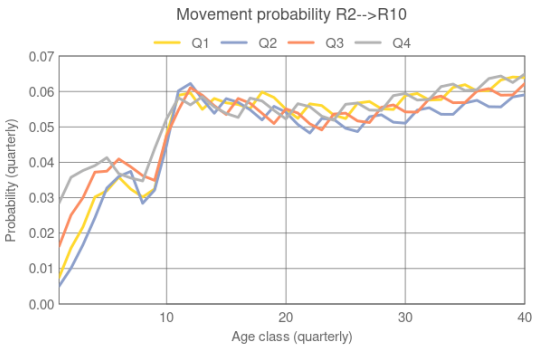

Region 2. Bigeye

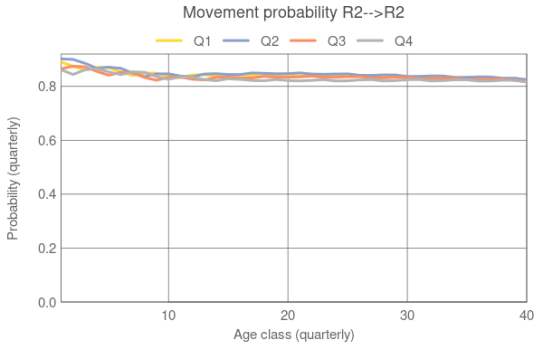

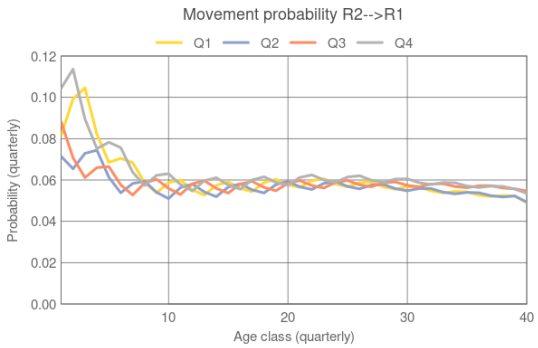

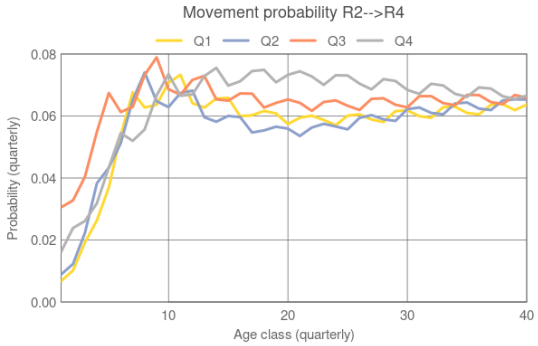

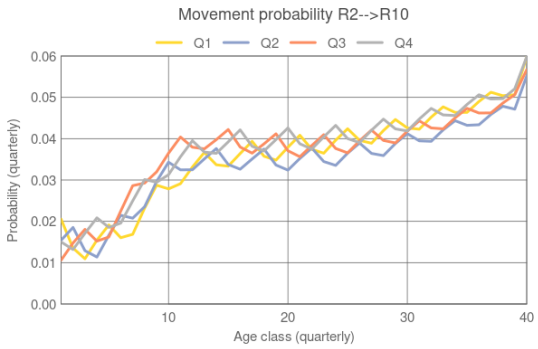

Figure 14: Regional movement probabilities from region 2 derived from SEAPODYM for the 9 Multifan-CL regions of "10N structure" (Vincent et al., 2020, Ducharme-Barth et al., 2020) and the EPO (shown as R10) region. Note, regions with all movement probabilities below 0.05 are not shown. Region R10 corresponds to the EPO region.

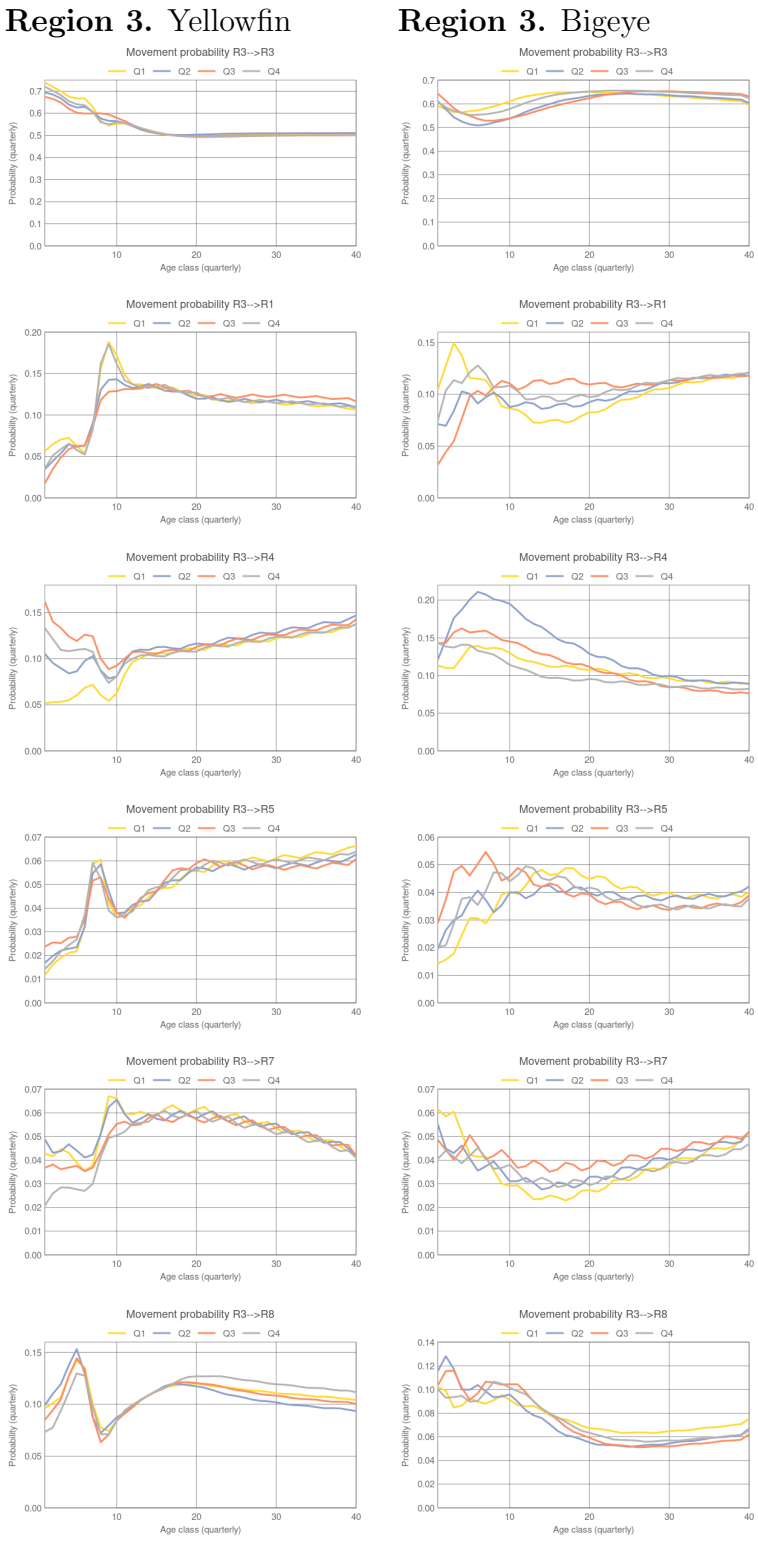

Figure 15: Regional movement probabilities from region 3 derived from SEAPODYM for the 9 Multifan-CL regions of "10N structure" (Vincent et al., 2020, Ducharme-Barth et al., 2020). Note, regions with all movement probabilities below 0.05 are not shown.

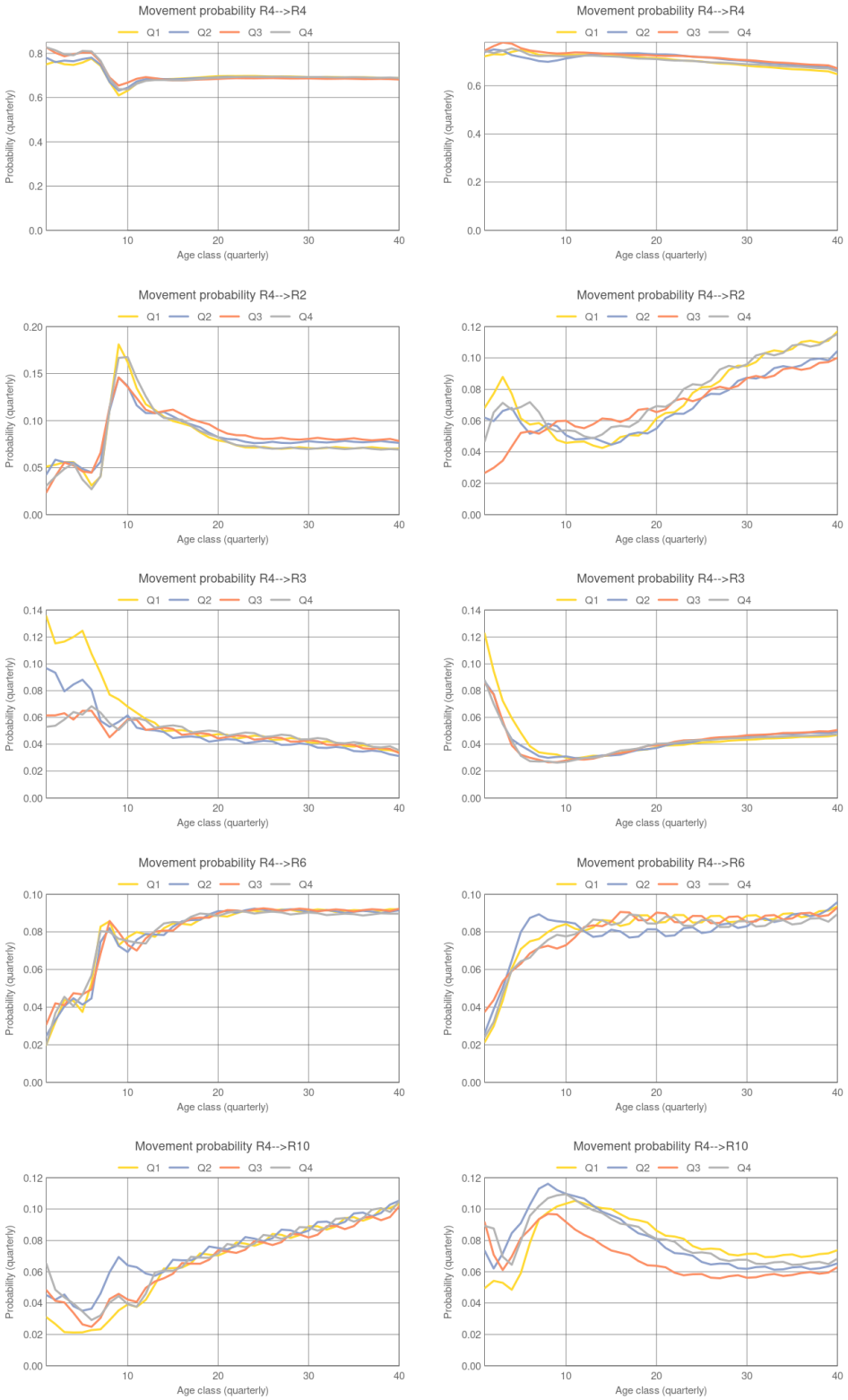

Figure 16: Regional movement probabilities from region 4 derived from SEAPODYM for the 9 Multifan-CL regions of "10N structure" (Vincent et al., 2020, Ducharme-Barth et al., 2020) and the EPO (shown as R10) region. Note, regions with all movement probabilities below 0.05 are not shown. Region R10 corresponds to the EPO region.

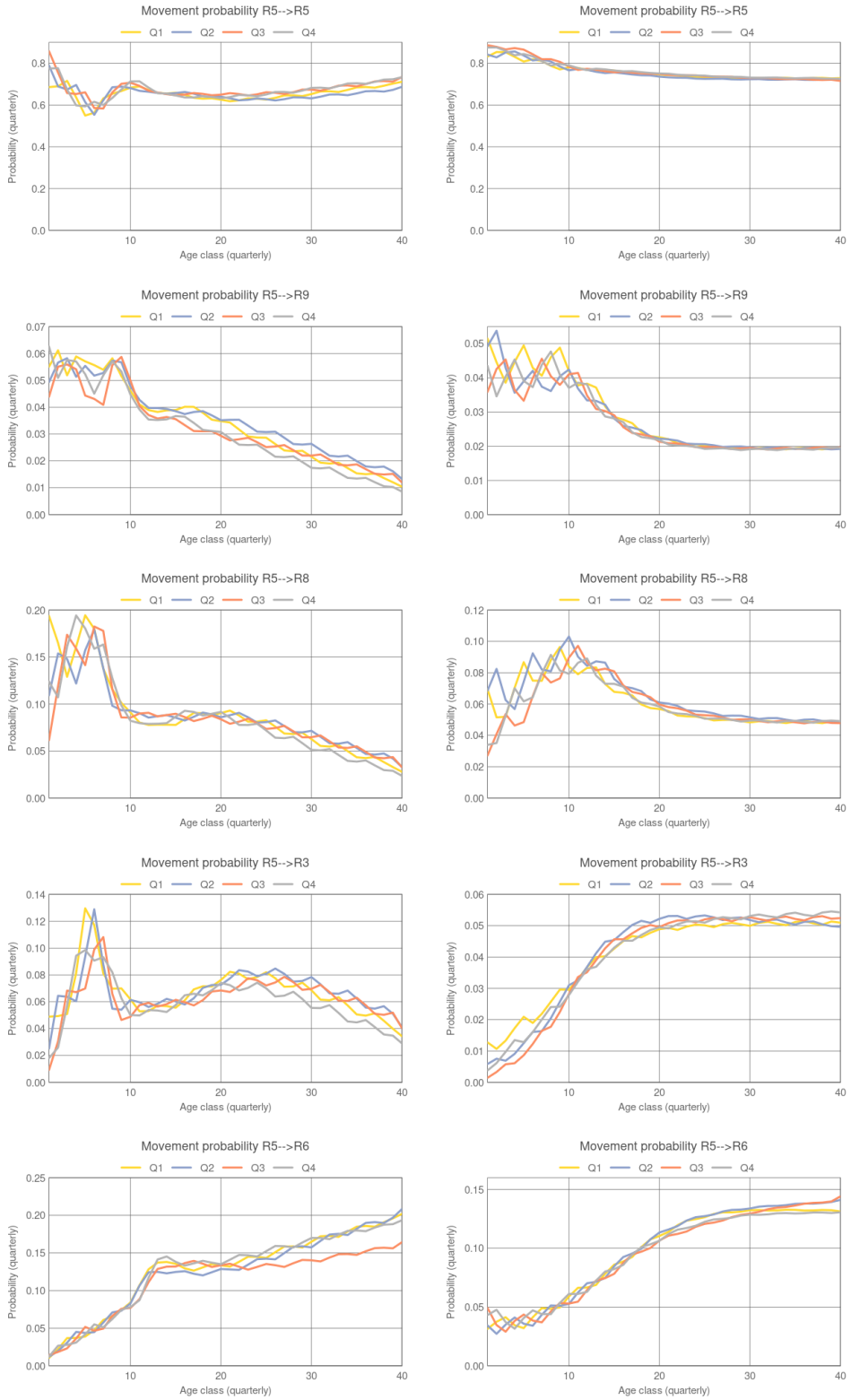

Figure 17: Regional movement probabilities from region 5 derived from SEAPODYM for the 9 Multifan-CL regions of "10N structure" (Vincent et al., 2020, Ducharme-Barth et al., 2020). Note, regions with all movement probabilities below 0.05 are not shown.

Region 6. Yellowfin

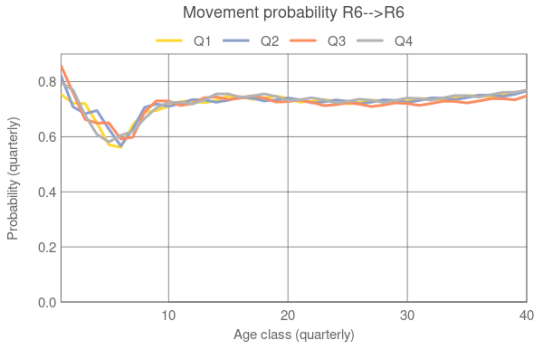

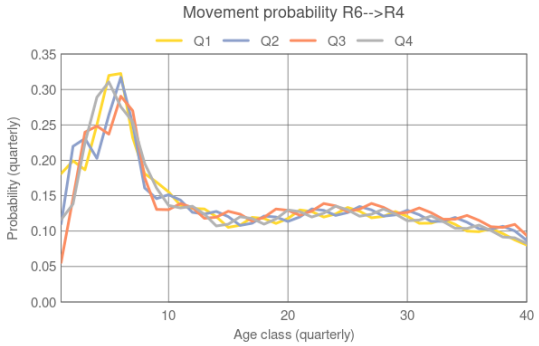

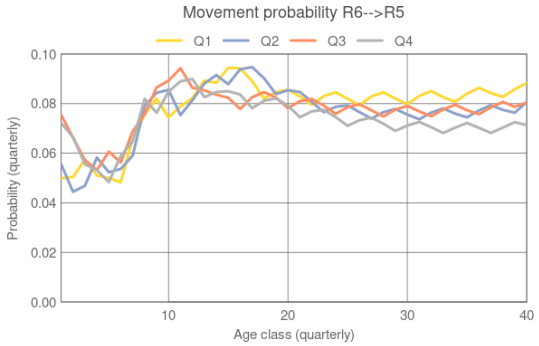

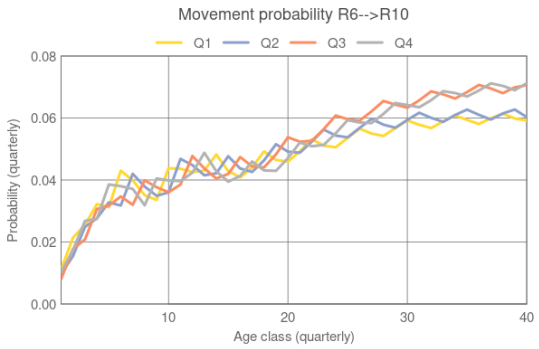

Region 6. Bigeye

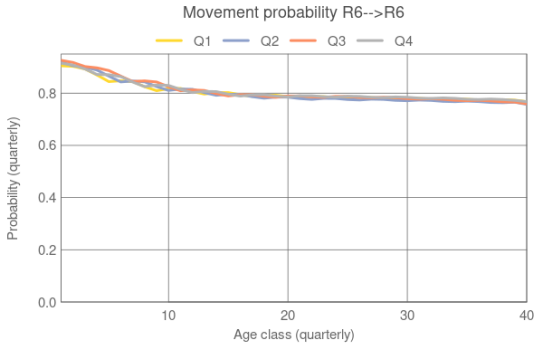

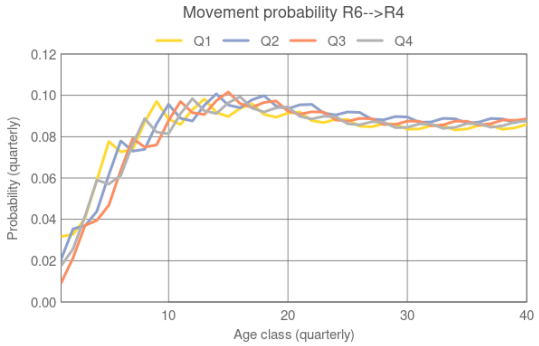

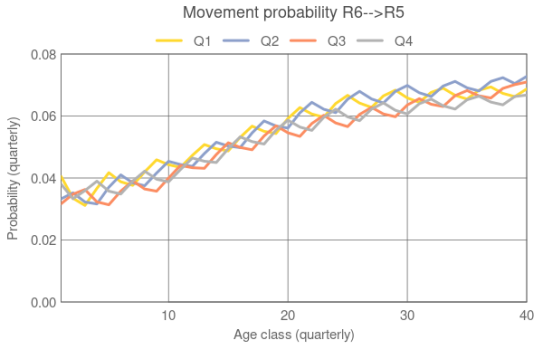

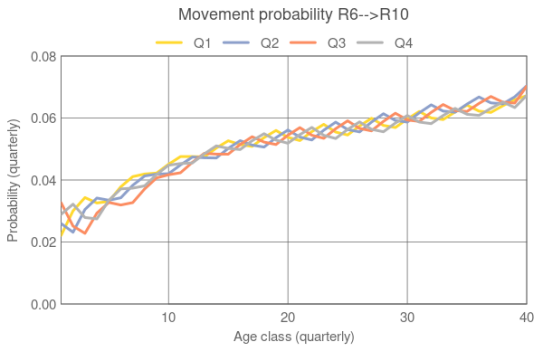

Figure 18: Regional movement probabilities from region 6 derived from SEAPODYM for the 9 Multifan-CL regions of "10N structure" (Vincent et al., 2020, Ducharme-Barth et al., 2020) and the EPO (shown as R10) region. Note, regions with all movement probabilities below 0.05 are not shown.

Region 7. Yellowfin

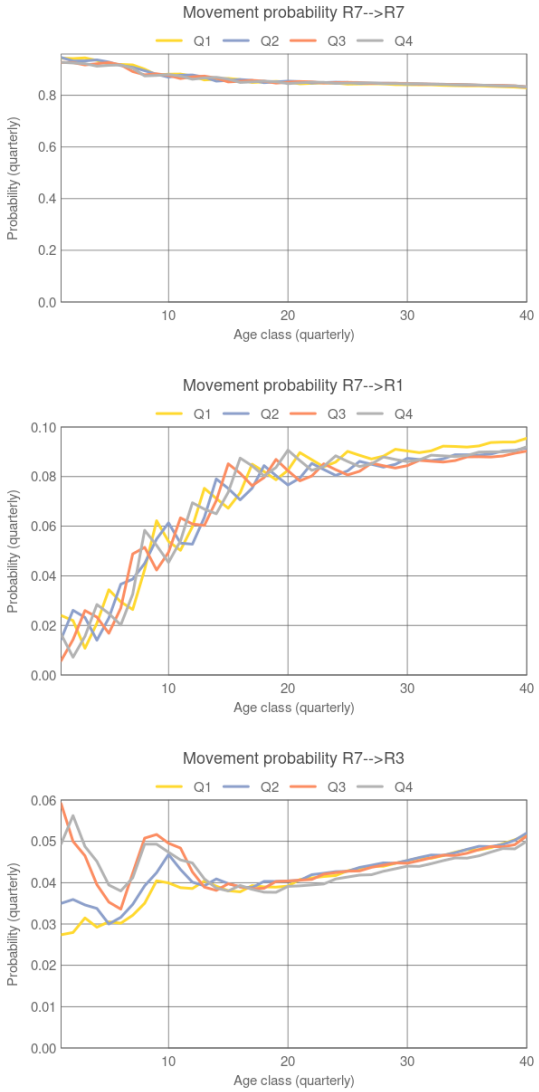

Region 7. Bigeye

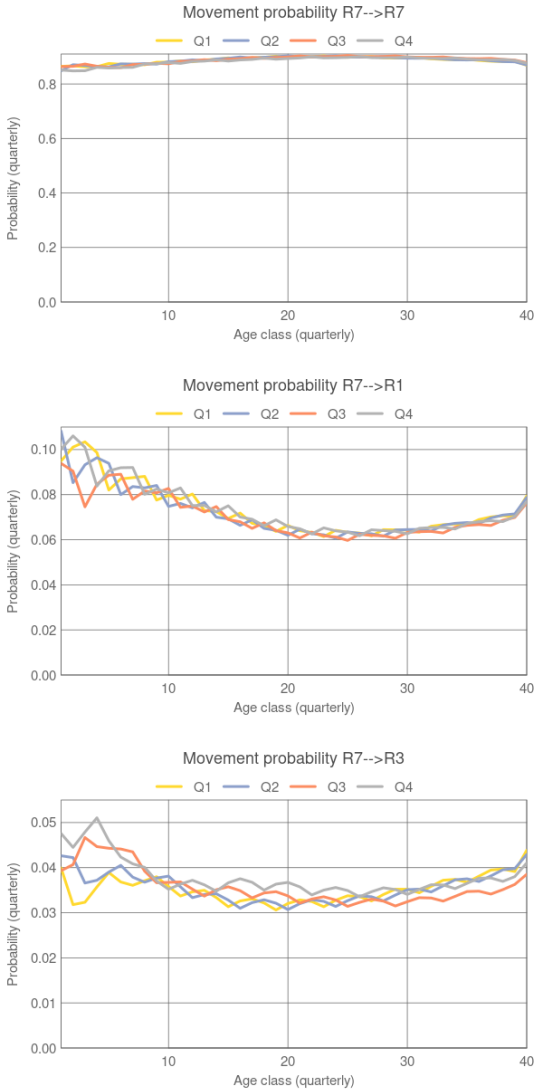

Figure 19: Regional movement probabilities from region 7 derived from SEAPODYM for the 9 Multifan-CL regions of "10N structure" (Vincent et al., 2020, Ducharme-Barth et al., 2020). Note, regions with all movement probabilities below 0.05 are not shown.

Region 8. Yellowfin

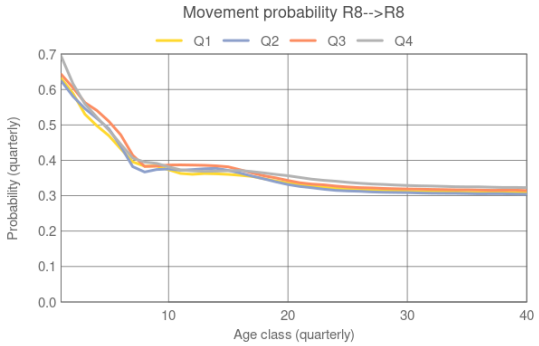

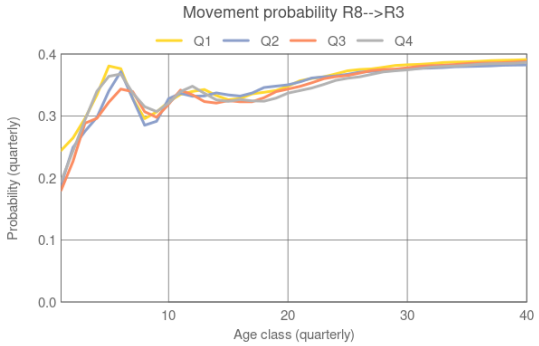

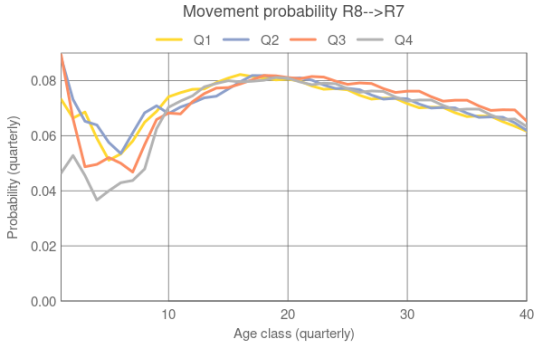

Region 8. Bigeye

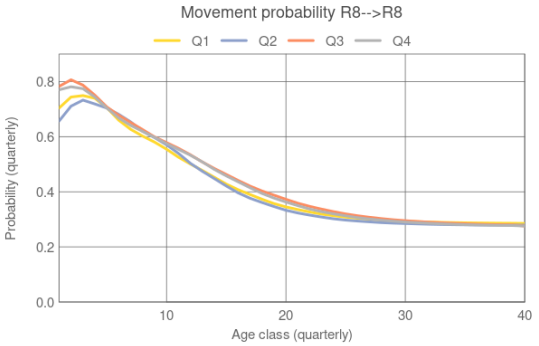

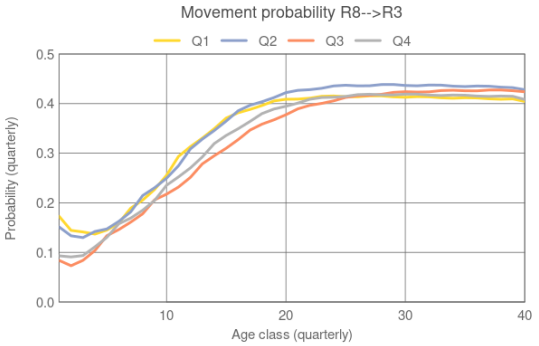

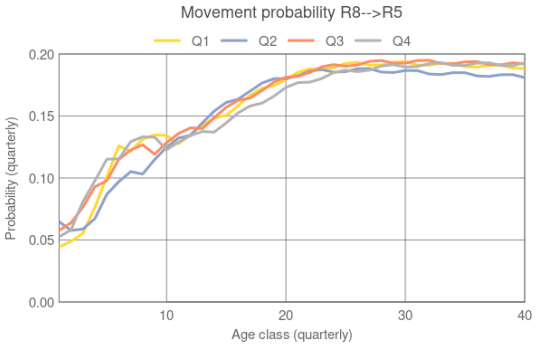

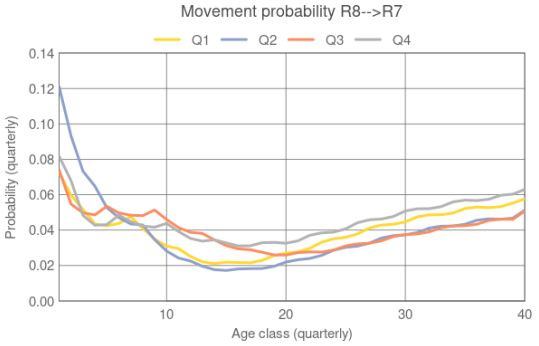

Figure 20: Regional movement probabilities from region 8 derived from SEAPODYM for the 9 Multifan-CL regions of "10N structure" (Vincent et al., 2020, Ducharme-Barth et al., 2020). Note, regions with all movement probabilities below 0.05 are not shown.

Region 9. Yellowfin

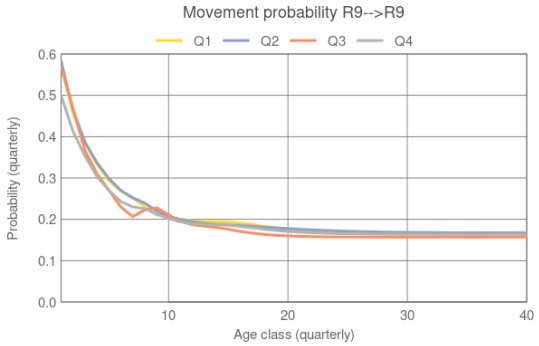

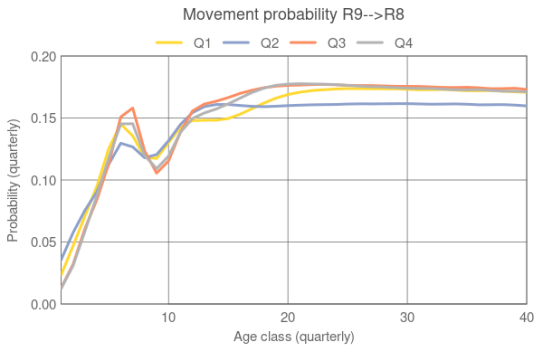

Region 9. Bigeye

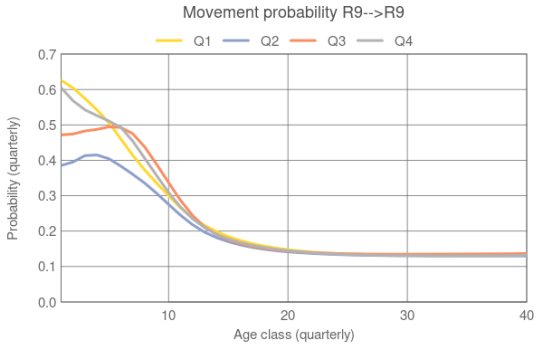

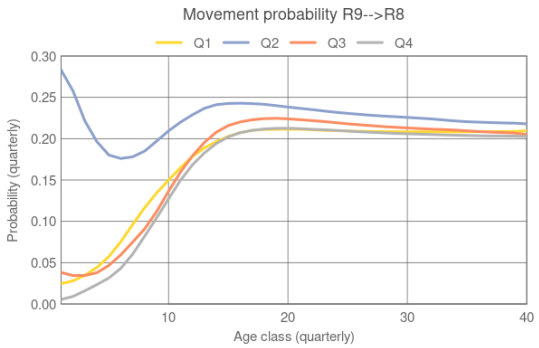

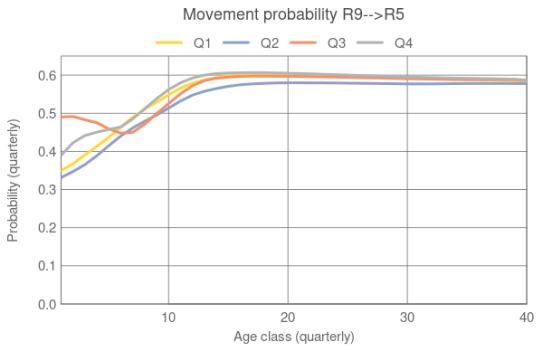

Figure 21: Regional movement probabilities from region 9 derived from SEAPODYM for the 9 Multifan-CL regions of "10N structure" (Vincent et al., 2020, Ducharme-Barth et al., 2020). Note, regions with all movement probabilities below 0.05 are not shown.

Appendix A: From SEAPODYM biomass flow rates to Multifan-CL movement probabilities

Let $B_{a,t,x,y}$ be the biomass density (in mt/km^2) of tuna population at age $a = 1, ..., A+$, time t and grid cell (x, y). Let's consider two regions, r_1 and r_2 and omit indices of age and time for simplicity. For a given age a, we denote

$$\beta_{r_1,r_2} = \sum_{i,j \in r_2} B_{t+\Delta t,x,y} \cdot \mathrm{A}_{xy}, \text{ when } B_{t,x,y}\ \forall x, y \in r_1 \text{ at time } t, \tag{1}$$

where A_{xy} is the grid cell surface area in km^2. Hence, we define β_{r_1,r_2} as the total regional biomass of one age class moving from region r_1 to region r_2 during time period $(t, t+\Delta t)$.

For a given age a, the time period t and for n regions, we have $n \times n$ matrix with all elements corresponding to the same time $t + \Delta t$:

$$\mathbf{F}_{a,t} = \begin{pmatrix} \beta_{1,1} & \beta_{1,2} & \dots & \beta_{1,n} \\ \beta_{2,1} & \beta_{2,2} & \dots & \beta_{2,n} \\ \vdots & \vdots & \vdots & \vdots \\ \beta_{n,1} & \beta_{n,2} & \dots & \beta_{n,n} \end{pmatrix}, \tag{2}$$

where the $\sum_j \beta_{i,j}$ is the total biomass that was in region i at time t, i.e., before the movement occurred, and the $\sum_i \beta_{i,j}$ is the biomass in region j after the movement occurred, i.e., the biomass in region j at time $t + \Delta t$. In other words,

$\sum_{j!=i} \beta_{i,j}$ – **outgoing biomass** from region i to other regions,

$\sum_{i!=j} \beta_{i,j}$ – **incoming biomass** to region j from other regions, and

β_{ii} – the **resident biomass** that stayed in the region i during the time interval $(t, t + \Delta t)$.

As seen from above, the elements of matrix $\mathbf{F}_{a,t}$ have units of mass flow rate, i.e., mt/Δt. In current SEAPODYM implementation, Δt is set to 3-months period, hence the original β_{ij} units are mt/qtr.

To convert the regional biomass flow rates to probabilities, we first convert the biomass to the number of individuals, which is necessary for the aggregation of several monthly age classes into a coarser Multifan-CL age structure. Simply using the mean weight-at-age $w(a)$ for each age class with mean age a, the total number of individuals moving from region i to j is $\nu_{a,t,i,j} = \frac{\beta_{a,i,j}}{w(a)}$. Then, the SEAPODYM flow rates are summed up to the Multifan-CL age classes α and averaged to the climatological quarters, resulting in $\nu_{\alpha,q,i,j} = \frac{1}{n} \sum_{t=q} \sum_{a \in \alpha} \nu_{a,t,i,j}$ in units Nb/qtr, where n is the number of years in the model run.

Then for a given age class α and a quarter q, the probability $p_{i,j}$ for the regional abundance to move from region i to region j during a quarterly time interval is computed as

$$p_{i,j} = \frac{\nu_{i,j}}{\sum_j \nu_{i,j}}, \tag{3}$$

where the sum in the denominator is the total number of individuals in region i before the movement occurred.

Finally, to match the Multifan-CL format, the movement matrices that are provided to the Multifan-CL model are the transpose of SEAPODYM-derived $\mathbf{P}_{\alpha,q}$ matrices with elements (3) such as:

$$\mathbf{P}^{\mathrm{T}}{}_{t,a} = \begin{pmatrix} p_{1,1} & p_{2,1} & \cdots & p_{n,1} \\ p_{1,2} & p_{2,2} & \cdots & p_{n,2} \\ \vdots & \vdots & \vdots & \vdots \\ p_{1,n} & p_{2,n} & \cdots & p_{n,n} \end{pmatrix}, \tag{4}$$

so the sum over each column of $\mathbf{P}^{\mathrm{T}}{}_{\alpha,q}$ is $\sum_j p_{i,j} = 1$.

Appendix B: CPUE of juvenile bigeye

a) Longline fleets targetting bigeye (Japan and Korea)

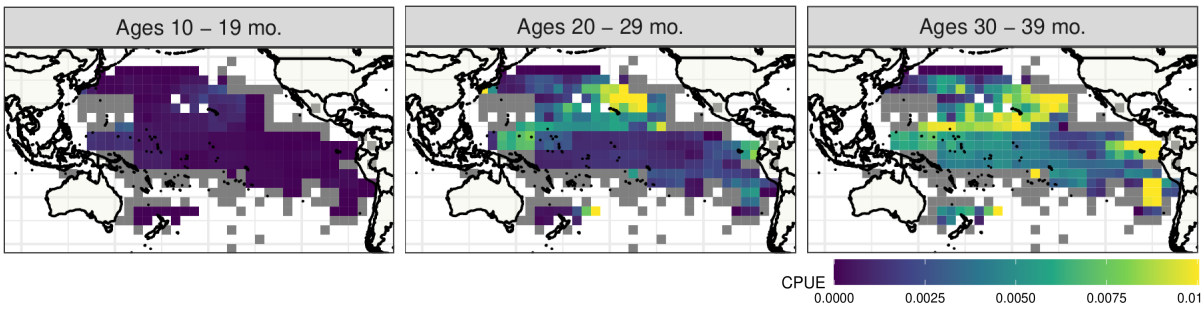

b) Asian longline fleets targetting albacore

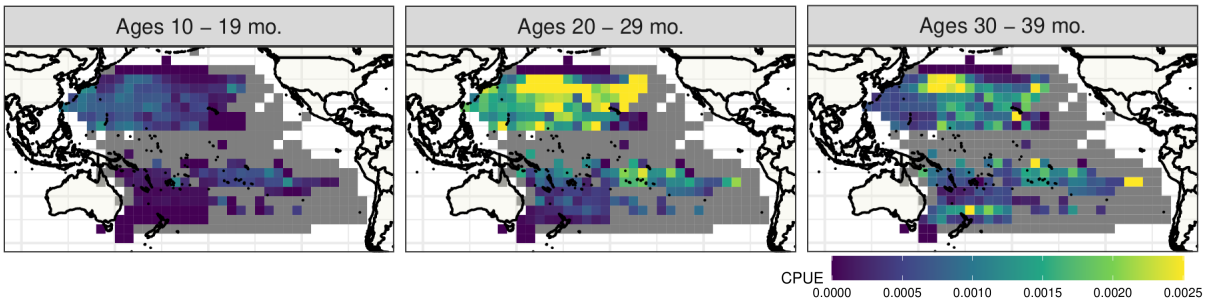

c) Pacific Islands longline fleets targetting bigeye

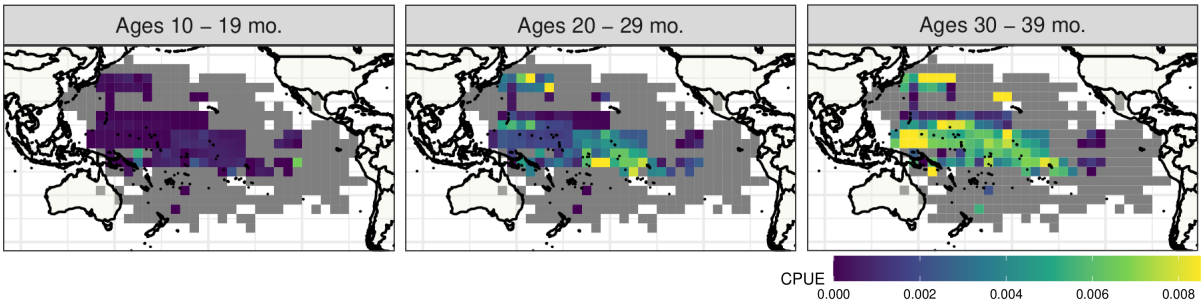

d) Pacific Islands longline fleets targetting albacore

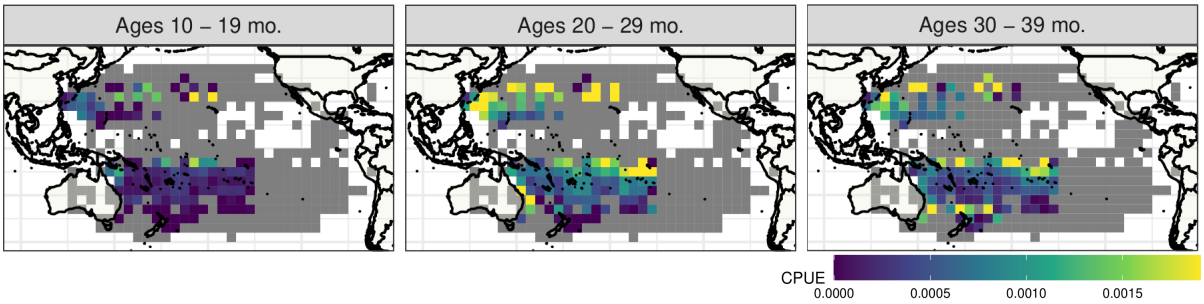

Figure B1: Longline CPUE (mt/100 hooks) of selected fisheries by age groups including juvenile and sub-adult bigeye. The mean sizes of selected age groups are 47-78 cm at 10-19 months, 78-103 cm at 20-29 months and 103-121 cm at 30-39 months. The mean size at 50% maturity, which defines the first adult class in SEAPODYM, is 115.7 cm.

a) Purse-seine fleets in WCPO with log sets

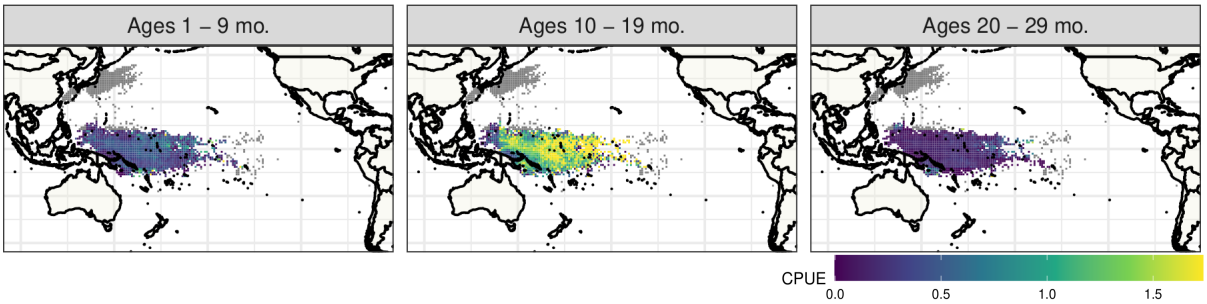

b) Purse-seine fleets in WCPO fishing at FADs

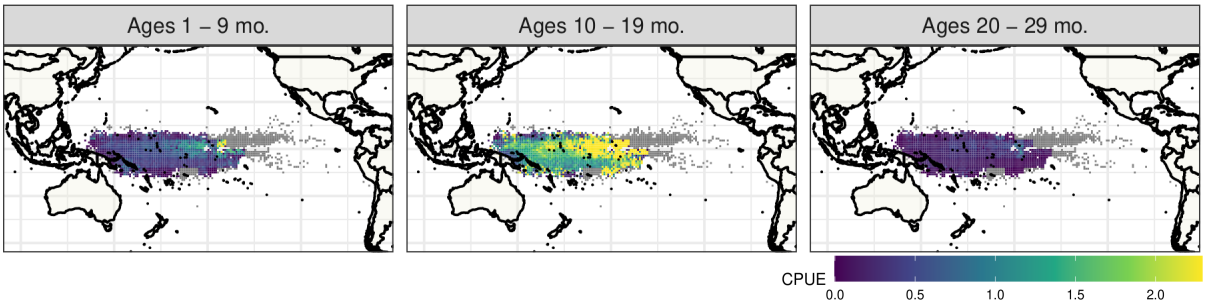

c) Purse-seine fleets in central and Eastern Pacific ocean fishing at FADs

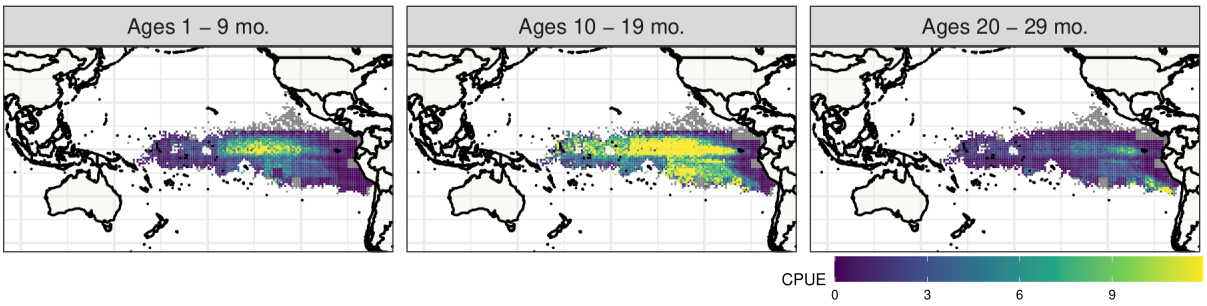

d) Pole-and-line fleets

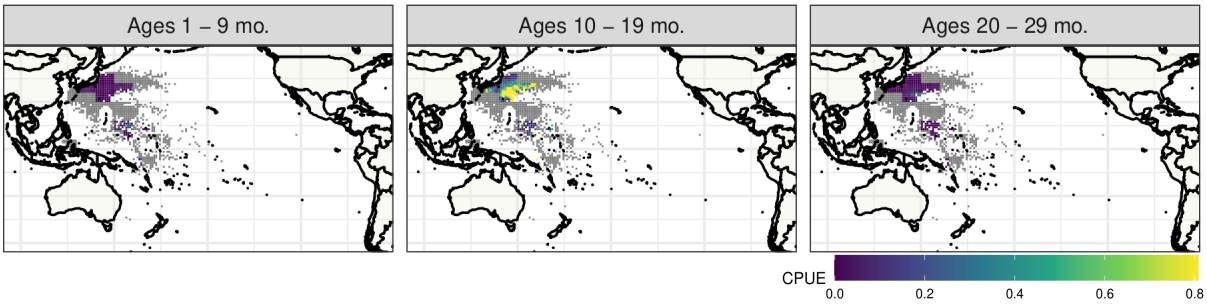

Figure B2: Surface gears CPUE (mt/days) of juvenile bigeye. The mean sizes of selected age groups are 13-47 cm at 1-9 months, 47-78 cm at 10-19 months, and 78-103 cm at 20-29 months.